UNIVERSIDAD POLITECNICA DE VALENCIA

TELECOM ESCUELA TÉCNICA VLC SUPERIOR DE UPV INGENIEROS DE TELECOMUNICACIÓN

VLC PHOTONICS

Photonics Research Labs

Reconfigurable Reflective Sagnac Interferometer in Si_3N_4

Author: Juan Fernández Vicente
Director: Pascual Muñoz Muñoz
Co-Director: José David Doménech Gómez

Resumen
En este trabajo se ha modelado, diseñado y testeado un reflectómetro de Sagnac reconfigurable para su uso como espejo varibale. Para hacer este dispositivo se ha realimentado dos configuraciones distintas de Mach-Zehnder, con una entrada o con dos entradas. Se han descrito matemáticamente para su análisis teórico ideal y se ha comparado los Mach-Zehnder con los reflectómetros de Sagnac. También se ha estudiado distintas variaciones y como afectan a su comportamiento respectivamente. Además, se ha diseñado un divisor siguiendo un nuevo esquema de diseño y se ha comprobado su mejora respecto a uno sin tenerlo en cuenta. Por otra parte, se ha diseñado un circuito integrado fotónico para el test de las diferentes estructuras en una plataforma de nitruro. A pesar de ciertas dificultades detectadas por un comportamiento no descrito en esta tecnologíao, se han obtenido resultados del circuito fabricado comprobando el correcto funcionamiento de los divisores y el resultado de las medidas activas acordes a lo estudiado teóricamente.

Resum
En aquest treball s'ha modelat, dissenyat i testeat un reflectómetre de Sagnac reconfigurable per al seu ús com a espill varibale. Per a fer aquest dispositiu s'ha realimentat dues configuracions diferents de Mach-Zehnder, amb una entrada o amb dues entrades. S'han descrit matemàticament per a la seua anàlisi teòrica ideal i s'ha comparat els Mach-Zehnder amb els altres reflectómetres de Sagnac. També s'ha estudiat diferents variacions i com afecten el seu comportament respectivament. A més, s'ha dissenyat un divisor seguint un nou esquema de disseny i s'ha comprovat la seua millora respecte a un sense tindre-ho en compte. D'altra banda, s'ha dissenyat un circuit integrat fotònic per al test de les diferents estructures en una plataforma de nitrur. Malgrat certes dificultats detectades per un comportament no descrit en aquesta tecnologia, s'han obtingut resultats del circuit fabricat comprovant el correcte funcionament dels divisors i el resultat de les mesures actives concordes a l'estudiat teòricament.

Abstract
In this work, a reconfigurable Sagnac reflectometer to use as a tunable mirror has been modelled, designed and tested. To make this device, two Mach-Zehnder configurations have been fed back, with one input or with two inputs. They have been described mathematically for their ideal theoretical analysis and the Mach-Zehnder has been compared with Sagnac reflectometers. Moreover, a study changing the parameters due to fabrications variations is made. On the other hand, a multimode interferometer splitter has been designed following a new design flow and its improvement has been checked. Furthermore, a photonic integrated circuit has been designed for the test of the different structures in a nitride platform. In spite of certain difficulties detected by a behaviour didn't describe in this technology, some results have been obtained from the fabricated circuit, verifying with the theory the right operation of the splitters and the active measurements.

Index

1. Introduction **2**

2. Objectives **2**

3. Methodology **3**

4. Modelling **4**
4.1. 3-ports and 4-ports networks . . . 4
4.1.1. 3-ports Networks . . . 4
4.1.2. 4-ports Networks . . . 5
4.1.3. S-matrix for integrated photonic elements . . . 7
4.2. Splitters . . . 7
4.2.1. Y-junction . . . 7
4.2.2. Multimode Interferometer (MMI) . . . 7
4.2.3. Directional coupler . . . 8
4.2.4. Star couplers . . . 9
4.2.5. General formulas . . . 9
4.3. Waveguides and Phase shifters . . . 10
4.4. Mach-Zehnder Interferometer . . . 10
4.5. Sagnac reflectors . . . 12

5. Simulations **13**
5.1. MZI vs Reflective Sagnac . . . 13
5.1.1. Tuning response of phase shifters: control of Amplitude and Phase 15
5.1.2. Changing excess loss and propagation losses . . . 18
5.2. Splitter design . . . 21
5.2.1. Material and Fabrication specifications . . . 22
5.2.2. Final designs . . . 22

6. Testing **23**
6.1. Passive Measurements . . . 24
6.2. Active Measurements . . . 27

7. Conclusions and Future work **29**

8. Acknowledgments **29**

9. Bibliography **29**

A. Additional measurement results **37**

Figures Index

1. Time Plan . . . 3
2. Schematic of 3-ports networks . . . 5
3. Schematic of 4-ports networks . . . 5
4. Schematic of MZI . . . 11
5. Schematic of a basic 2x2 Reflective Sagnac . . . 12
6. Schematic of 1x2 MZI, MZI2x2, Reflective Sagnac 2x2 and Reflective Sagnac 1x2 . . . 14
7. Comparative figure between 2x2 MZI and RSL 2x2. Transmision of MZI in the cross-port (solid blue line), transmision of MZI in the direct-port (dots blue line), transmision of RSL (solid red line), reflection of RSL (dots red line). . . . 15
8. Comparative figure between 1x2 MZI and RSL 1x2. Transmision of MZI in the cross-port (solid blue line), transmision of MZI in the direct-port (dots blue line), reflection of RSL (dots red line). . . . 16
9. Comparative figure between 2x2 MZI and RSL 2x2 adding phase in both arms. Transmision of MZI in the cross-port (solid blue line), transmision of MZI in the direct-port (dots blue line), transmision of RSL (solid red line), reflection of RSL (dots red line). . . . 17
10. Comparative figure between 1x2 MZI and RSL 1x2 adding phase in both arms. Transmision of MZI in the cross-port (solid blue line), transmision of MZI in the direct-port (dots blue line), reflection of RSL (solid red line). 18
11. Comparative figure between 2x2 MZI and RSL 2x2 changing excess loss and propagation losses. Transmision of MZI in the cross-port (solid blue line), transmision of MZI in the direct-port (dots blue line), transmision of RSL (solid red line), reflection of RSL (dots red line). . . . 19
12. Comparative figure between 1x2 MZI and RSL 1x2 changing excess loss and propagation losses. Transmision of MZI in the cross-port (solid blue line), transmision of MZI in the direct-port (dots blue line), reflection of RSL (solid red line). . . . 20
13. Bouncing behaviour of the MMI output images . . . 21
14. Schematic of Deep and Shallow waveguide . . . 22
15. Die design 5.5x5.5 mm^2 . . . 23
16. Setup . . . 24
17. Measurements normalized of the output distribution of 2x2 MMI of 8.4 µm width. . . . 25
18. Measurements normalized of the output distribution of 2x2 MMI of 11.4 µm width. . . . 25
19. Measurements normalized of the output distribution of 1x2 MMI of 8.4 µm width. . . . 26
20. Measurements normalized of the output distribution of 1x2 MMI of 11.4 µm width. . . . 26
21. Photonic integration Chip on PCB . . . 27

22. MZI versus RSL with 2x2 MMI. 28
23. MZI versus RSL with 1x2 MMI. 28
24. Normalized measurements the 2x2 MMI of 8.4 µm width outputs. 38
25. Excess losses of the 2x2 MMI of 8.4 µm width. 39
26. Normalized measurements the 2x2 MMI of 11.4 µm width outputs. 40
27. Excess losses of 2x2 MMI of 11.4 µm width. 41
28. Normalized measurements the 1x2 MMI of 8.4 µm width outputs. 42
29. Excess losses of 1x2 MMI of 8.4 µm width. 43
30. Normalized measurements the 1x2 MMI of 11.4 µm width outputs. 44
31. Excess losses of 1x2 MMI of 11.4 µm width. 45
32. MZI versus RSL of 11.4 µm width MMIs. RSL Reflection (MMI1x2) or Transmision (MMI2x2) (blue), MZI Cross-port (red) and MZI Direct-port (yellow) 46
33. MZI versus RSL of 8.4 µm width MMIs. RSL Reflection (MMI1x2) or Transmision (MMI2x2) (blue), MZI Cross-port (red) and MZI Direct-port (yellow) 47

1. Introduction

Photonics is the branch of physics that deals with the properties and applications of photons, especially for the transmission of information covering the entire spectrum from the ultraviolet to the infra-red. It started with the creation of a stable and coherent light source called laser. In the following developments, communications through the atmosphere were first attempted, and it was discovered that transmission was very sensitive to the changes in the environment. For this reason, guided optics solution was approached, in which a material conducive the light trough the medium is used for communication, analogously to electronics and, by extension, to microelectronics. The application of the same scale size of microelectronics applied to optics is named integrated optics. The term of integrated optics was coined in 1969 by [1, 2] to describe all those integrated circuits that worked with the manipulation of photons. In this manipulations of the optics and integrate bulky optical systems, the spectrometers are one of the most promising applications. In the optical applications the spectra are acquired with costly off-chip bulky instruments (such as tunable lasers combined with photo-detectors, or broad band sources with optical spectrum analyzers). Hence, it is clear than bringing into the chip area a spectrometer will complement and suppose a significant progress over the current state of the art of photonic chip sensors, in the line of current trends on wearable chip sensors technologies. This project departs from the very recent research seed result, reported by the photonics research lab team on Reflective Arrayed Waveguide Gratings (R-AWG) [3]. The concept, theoretical description, and very first basic experimental demonstration of a Silicon-on-Insulator (SOI) R-AWG static spectrometer were reported for the telecom C-band (wavelength range of 1530-1565 nm). The AWG is a very well-known device, principally applied to wavelength division multi-/de-multiplexing in telecom networks [4]. A R-AWG is half of a standard AWG, where mirrors are included half-way the arms, so it operates in reflective mode, leading to approximately half of the footprint. The mirrors in this concept [3] are implemented via Sagnac Loop Reflectors (SLRs), whose response maybe adjusted by means of variable optical couplers. These couplers can be implemented for broadband operation and fabrication reproducibility, by means of Mach-Zehnder based broad-band, phase shift enabled.
The aim of this work is to study the different models of Reflective Sagnac trying to implement the response of this device as a tunable mirror. The approach of this work is to study what is the best solution to implement reflectors using elements with 2 inputs and 2 outputs (4-ports) or elements with 1 input and 2 outputs (3-ports).

2. Objectives

The main objective of this work is the design of reflective Sagnac loops and understanding their response. The final goal is to use it in other structures to obtain tunable response as in R-AWG [3]. Also, this works pretends to be a reference of this type of devices in integrated optics as tunables mirrors. Another objective of this work is to develop the mathematical formalism to analyse this device in a system to be integrated in the

future with other devices.

3. Methodology

To reach the objectives, the full work was divided in different tasks. The order followed in the development of this work is summarized below.

1. Study of the formulas of the Reflective Sagnac Loop. A literature study has been made to fit appropriate formalism for the structure.
2. Development of the mathematical code and cross-check with theoretical study.
3. Design of the splitters. Analysis of the different implementations available. A 1x2 MMI and a 2x2 MMI were designed following a novel design flow.
4. Design of the full die 5x5 for the MPW of CNM [5].
5. Characterization of the dies and corroboration of the theoretical assumptions..
6. Writing of the final document.

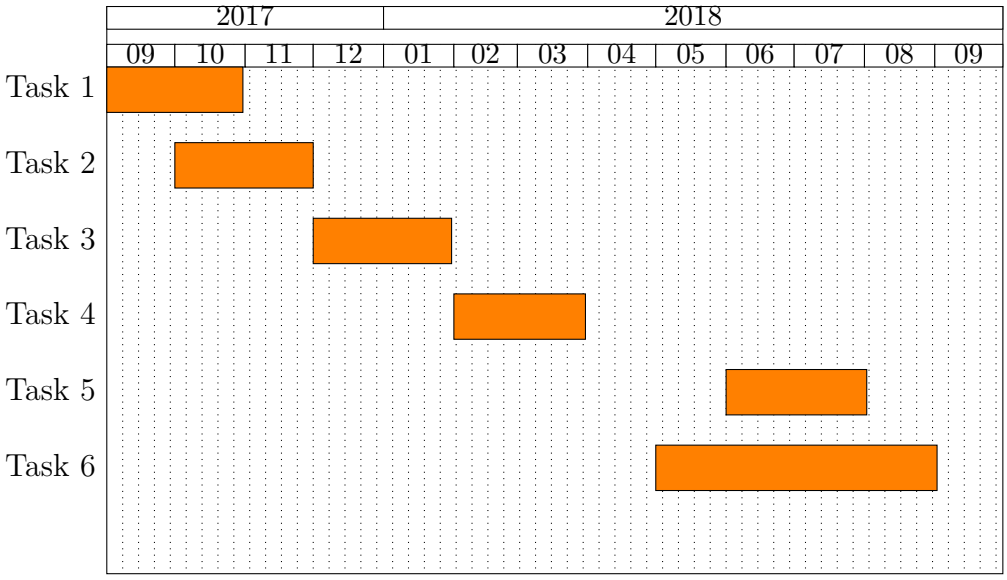

Figure 1: Time Plan

4. Modelling

Photonic devices can be studied as S-matrix networks like in microwave world [6]. A remarkable feature of S-matrix is the possibility to change to transfer matrix formalism to operate iteratively with mathematical programs to obtain the total response of the device [7].

However, one of the major drawbacks to adopt this formalism are the 3-ports networks. The optical connections supports polarization, spatial and temporal modes. In contrast with electrical connections, optics can support two polarization modes and many spatial modes. It cannot violate the second law of the thermodinamics, but optical systems can support many spatial modes and two polarization modes that can be devised to combine beams without loss[8]. This property allows to introduce some changes in the 3-ports networks.

Consequently, a study of the 3 and 4 ports elements in integrated photonics is made. To conclude, the Sagnac Loop reflectors formulation is developed.

4.1. 3-ports and 4-ports networks

For this work we are interested in two types of devices: 3-ports networks and 4-ports networks. There are three important properties of S-matrix: reciprocity, matched ports and lossless.

Reciprocity is a property that depends on the materials employed in the integration technology. The typical platforms like InP, SOI and Si_3N_4 employ reciprocal materials. The matching of the ports depends on the impedance that the optical wave 'sees' when arriving to the output port. The impedance of a wave in photonics follows the same idea as in electronics. In this case the impedance of an electromagnetic wave with a specific power distribution (mode solution of a waveguide) in optics depends on the effective index. This effective index is proportional to the width of waveguide if the other parameters remain ideally constant as height of the waveguide, the angle of the facets, the roughness of the facets and the refractive index of the materials. This parameter gives an idea of the reflections that could be due to abrupt changes of the refractive indexes. Despite this, in integrated optics the reflections are low and in junctions can be neglected [9-14].

4.1.1. 3-ports Networks

Following the basic theory, these devices have the next S-Matrix and port definition:

$$\begin{pmatrix} S_{11} & S_{12} & S_{13} \\ S_{21} & S_{22} & S_{23} \\ S_{31} & S_{32} & S_{33} \end{pmatrix}$$

Figure 2: Schematic of 3-ports networks

Firstly, the reciprocal condition is evaluated. This device is passive and made of simple (isotropic) materials, it means that this device will be reciprocal. This condition constrain the elements of the matrix:

$$S_{21} = S_{12}, \quad S_{31} = S_{13}, \quad S_{23} = S_{32} \tag{1}$$

Secondly, these networks don't produce any reflections, they are matched, so it can be translated to:

$$S_{11} = S_{22} = S_{33} = 0 \tag{2}$$

And finally, if this network has to be lossless (all input power is distributed to the output), the scattering matrix must be unitary, and therefore:

$$\begin{aligned} |S_{21}|^2 + |S_{31}|^2 &= 1 \qquad S_{31}^* S_{32} = 0 \\ |S_{21}|^2 + |S_{32}|^2 &= 1 \qquad S_{21}^* S_{32} = 0 \\ |S_{31}|^2 + |S_{32}|^2 &= 1 \qquad S_{21}^* S_{31} = 0 \end{aligned} \tag{3}$$

We can conclude that for 3-port networks, the three conditions cannot be fullfilled at the same time.

4.1.2. 4-ports Networks

Following the basic theory, these devices have the next S-Matrix and port definition:

$$\begin{pmatrix} S_{11} & S_{12} & S_{13} & S_{14} \\ S_{21} & S_{22} & S_{23} & S_{24} \\ S_{31} & S_{32} & S_{33} & S_{34} \\ S_{41} & S_{42} & S_{43} & S_{44} \end{pmatrix}$$

Figure 3: Schematic of 4-ports networks

These networks can be reciprocal, matched and lossless. It can be simplified all the conditions with the next formulas:

$$S_{ij} = S_{ji} \tag{4}$$
$$S_{ii} = 0 \tag{5}$$
$$|S_{13}|^2 = |S_{24}|^2 = A^2 \tag{6}$$
$$|S_{12}|^2 = |S_{34}|^2 = B^2 \tag{7}$$
$$S_{14} = S_{23} = 0 \tag{8}$$
$$\alpha_{12} - \alpha_{13} = \alpha_{24} - \alpha_{34} + \pi \tag{9}$$

Renaming the input and output ports as:: 1'=1, 2'=3, 3'=4, 4'=2, we can obtain two generic solutions:
(1) Symmetric coupler

$$\begin{pmatrix} 0 & 0 & B & jA \\ 0 & 0 & jA & B \\ B & jA & 0 & 0 \\ jA & B & 0 & 0 \end{pmatrix}$$

(2) Antisymmetric coupler

$$\begin{pmatrix} 0 & 0 & B & A \\ 0 & 0 & -A & B \\ B & -A & 0 & 0 \\ A & B & 0 & 0 \end{pmatrix}$$

Once the solutions are obtained we can describe the matrix formalism problem. The array vector a_i contains the input electromagnetic waves of each i port. On the other hand, the array vector of b_i contains the output electromagnetic waves of each i port.

$$\begin{pmatrix} b1 \\ b2 \\ b3 \\ b4 \end{pmatrix} = \begin{pmatrix} 0 & 0 & S_{13} & S_{14} \\ 0 & 0 & S_{23} & S_{23} \\ S_{31} & S_{32} & 0 & 0 \\ S_{41} & S_{42} & 0 & 0 \end{pmatrix} * \begin{pmatrix} a1 \\ a2 \\ a3 \\ a4 \end{pmatrix}$$

With this configuration is easy to obtain the transfer matrix formalism. This formalism allows to obtain the complete solution of a complex system by multiplying the individual transfer matrices of the simple individual devices. This simple solution eases the implementation of the formalism in mathematical softwares.

$$\begin{pmatrix} a3 \\ b3 \\ a4 \\ b4 \end{pmatrix} = \begin{pmatrix} 0 & T_{12} & 0 & T_{14} \\ T_{21} & 0 & T_{23} & 0 \\ 0 & T_{32} & 0 & T_{34} \\ T_{41} & 0 & T_{43} & 0 \end{pmatrix} * \begin{pmatrix} a1 \\ b1 \\ a2 \\ b2 \end{pmatrix}$$

Interestingly, this scattering matrix gives an special treatment for these elements: the splicing of the matrix 4x4 in two scattering matrix 2x2, for the forward and backward direction [15]. This formalism simplified the study of the behaviour of integrated optics elements.

4.1.3. S-matrix for integrated photonic elements

In integrated optics there are three port elements as Y-juntions or 1x2 MMIs that will be further developed in the next section. These elements has special treatment in dielectric waveguides because they don't have reflections, are reciprocal and unitary (lossless). In the section 4.1.1 is shown that is not possible to satisfy all conditions. There were some works trying to explain this particular case [9-14]. As mentioned in the begining of this section this case is directly connected to the properties of optical waveguides that support diferent spatial modes[8].
In summary, the approach to analyse these elements is to decompose the input modes between two modes, the symmetric and antisymmetric modes. So, these supermodes are propagated along the structure until to the output port. The interference among them obtains two solutions depending on the inputs, the first mode and the radiation mode of the output waveguide [13]. Thus, the 3-ports elements can be converted as 4-ports element with an extra port due to radiation mode [12] and with this configuration the analysis is possible. Most of the elements in integrated optics can neglected the reflections due to this effect to couple to radiation modes.

4.2. Splitters

There are different structures to couple and split light. The most common structures are Y-branches, Directional Couplers, Star couplers and Multimode Interferometer (MMI). The next formalism of S-matrix only focus in 3 dB couplers but in the next sections we will generalize for all cases [16].

4.2.1. Y-junction

Y-branch is the first logical approach to try to split and couple light. The main characteristics are that it can be lossless ,fabrication tolerant ,compact and broadband [9-14]. Fabrication of the tip of the y-junction could be a problem in some technologies as higher index contrast technologies, that they could introduce reflections in the splitting due to the vertical position of the tip to the propagation of the light.

$$S = \frac{1}{\sqrt{2}} \begin{pmatrix} 0 & 0 & 1 & 1 \\ 0 & 0 & -1 & 1 \\ 1 & -1 & 0 & 0 \\ 1 & 1 & 0 & 0 \end{pmatrix}$$

4.2.2. Multimode Interferometer (MMI)

MMI [17, 18] is based in self-imaging. Self-imaging is a property of multi-mode waveguides by which an input field profile is reproduced in single or multiple images at periodic intervals along the propagation direction of the guide. This effect allows to build whatever NxN device that the designer wants (better explanation of MMI and images in [17]).

In multimode interferometers splitter, the facets of the elements could introduce some reflections due to the contrast of the index and the total internal reflection. There are some techniques trying to reduce the losses [19]. In high index contrast is a compact element with low insertion losses and it allows to design a splitter of the number of inputs and outputs desired. In low index contrast could be bigger than other splitters. It is an element that is less sensitive to fabrication tolerances and it has typical flat response over a broad wavelength range.

MMI-2x1 50/50

$$S = \frac{1}{\sqrt{2}} \begin{pmatrix} 0 & 0 & 1 & 1 \\ 0 & 0 & -1 & 1 \\ 1 & -1 & 0 & 0 \\ 1 & 1 & 0 & 0 \end{pmatrix}$$

This is the solution of antisymmetric 4-ports networks. If a radiation mode port is introduced, the matrix is unitary in both directions. In one direction divides the power and in the other direction combines the power. The power coupled to the radiated mode could also produce a propagation of higher order modes, degrading the optical response.

The 2x2 MMI is a symmetric splitter that introduces a phase shift of $\pi/2$ in the other output port.

MMI-2x2 50/50

$$S = \frac{1}{\sqrt{2}} \begin{pmatrix} 0 & 0 & 1 & j \\ 0 & 0 & j & 1 \\ 1 & j & 0 & 0 \\ j & 1 & 0 & 0 \end{pmatrix}$$

This device introduces a phase shift of $\pi/2$ if the length of the device is under L_{MMI}. Each L_{MMI} even , a same $\pi/2$ phase shift is obtained. Each L_{MMI} even , a -$\pi/2$ phase shift is obtained.

4.2.3. Directional coupler

Directional couplers are devices that are typically described employing the coupled mode theory. Applying perturbation theory it can be approximated the propagation of one waveguide as a symmetric and asymmetric mode. If both are excited, the exchange between them provides a specific distribution of the power at the output [1]. The simplest formulas of directional couplers can be extracted from [20], [21] and [22]. Yariv [20] shows the unitary matrix formalism of complex coeficients (that it englobes symmetric and antisymmetric solution) and [21] explains the steps to obtain the general solutions of a symmetric splitter.

Following the numbering of the ports

$$S = \frac{1}{\sqrt{2}} \begin{pmatrix} 0 & 0 & 1 & j \\ 0 & 0 & j & 1 \\ 1 & j & 0 & 0 \\ j & 1 & 0 & 0 \end{pmatrix}$$

Traditional design produces that any change in the gap, width, thickness or refractive index of the parallel waveguides could introduce big changes in the directional coupler behaviour. New design techniques have been developed to obtain less sensitive devices to fabrication tolerances like bent copuplers, adiabatic couplers, etc [16, 23]. The main advantages of this element is that introduce less insertion losses and polarization dependent losses (PDL) than MMIs and they are usually more compact [24].

4.2.4. Star couplers

Star couplers are based in the difraction of the optical beam when is launched in a free propagation region [25]. It is not an ideal splitter due to their working principle, some of the power is lost in the transformation between an expanded gaussian and optical modes of the waveguides at the output. It is a device that when the number of the outputs and inputs is high (more than 10) is a good candidate to combine and split power because the insertion losses and imbalance are lower than a cascade of splitters. Curiously, this element could be approximate as a spatial Fourier transform of input plane [26]. In fact, star coupler is a key element for the array waveguide grating that exploits this propiery of this element to filter and other applications [27-29].
Star coupler could be used as splitter and combiner but is more focused in wavelength dependent systems and it is bulky and it has more losses and imbalance if compares with other devices.

4.2.5. General formulas

As a summary there is one scattering matrix that generalizes the behaviour of splitters of 2 output ports and it will be used in this work.

$$S = \begin{pmatrix} 0 & 0 & t^* & k \\ 0 & 0 & -k^* & t \\ t^* & -k^* & 0 & 0 \\ k & t & 0 & 0 \end{pmatrix}$$

To simplify the problem and due to the zero reflections and crosstalk, this matrix 4x4 can be spliced in forward and backward matrices. Backward matrix is the transposed version of the forward matrix. Following the steps of [21], it is straightforward to verify the transfer matrix solution.

$$S_{forward} = S^T_{backward} = \begin{pmatrix} t^* & -k^* \\ k & t \end{pmatrix}$$

$$T_{forward} = T^T_{backward} = 1/\gamma \begin{pmatrix} t & k^* \\ -k & t^* \end{pmatrix} \tag{10}$$

In the ideal case of no losses the last equation will be 1, but to taking into account extra losses from to propagate lossy modes and other extra losses, a positive parameter is defined of the excess losses of the device ($1/\gamma$):

$$|k|^2 + |t|^2 = 1/\gamma \tag{11}$$

The reflections (the zero elements of the diagonal of the matrix) and the crosstalk (the rest of zero elements of the matrix) of the input optical ports can be neglected. By having this configuration, we are able to analyse the circuit in the forward and backward direction independently. The resulting matrix can be specified for both cases under the study. In the case of devices with 2 inputs and 2 outputs the formulas of elements of the matrix are:

$$k = j * \sqrt{K}, t = \sqrt{1 - K} \tag{12}$$

And in the case of 1 input and 2 outputs or vice-versa the formulas of elements of the matrix are:

$$k = \sqrt{K}, t = \sqrt{1 - K} \tag{13}$$

Being K the amount of power of the cross port .

4.3. Waveguides and Phase shifters

The input and output of one waveguide are related through the equation:

$$|E_f|_{in} = |E_f|_{out} \cdot e^{-\alpha L} \cdot e^{-j\beta L} |E_f|_{out} = |E_f|_{in} \cdot e^{\alpha L} \cdot e^{j\beta L} \tag{14}$$

Any change of β, the propagation constant, means a change in the material or how the mode is propagated. There are different ways to change the refractive index in a waveguide changing the real or imaginary part of the propagation constant. When the real part is changed (for instance by changing the temperature of the waveguides) a phase shift is produced. In contrast, when the imaginary part is changed, the losses of the propagated mode is modified.
In order to use the TMF in the Sagnac Loop a special multiplication has to be made because the forward and backward matrices of the element are connected. The transfer matrix takes into account the direction of the light for the forward direction (-j) or backward direction (j) [15]. The multiplication of the transfer matrices of a device and the loop is:

$$T_{system} = T_{device} -> T_{loop} = T_{loop} * T_{device_f} * T_{inv} * T_{device_b} \tag{15}$$

$$T_{loop} = \begin{pmatrix} e^{\alpha_2 + j\beta_2 L_2} & 0 \\ 0 & e^{-\alpha_2 - j\beta_2 L_2} \end{pmatrix} T_{inv} = \begin{pmatrix} 0 & 1 \\ 1 & 0 \end{pmatrix} \tag{16}$$

4.4. Mach-Zehnder Interferometer

The Mach-Zehnder Interferometer (MZI) is a simple device that demonstrates the interference by division of amplitude. The light is first split into two parts by a splitter. Depending on the relative phase acquired by the light along the two paths the second splitter will split proportionally the light between ports. A schematic description of a MZI is shown in Section 4.4. Employing the developments of subsection 4.2.5, it is easy to obtain the general formulas describing the MZI operation.

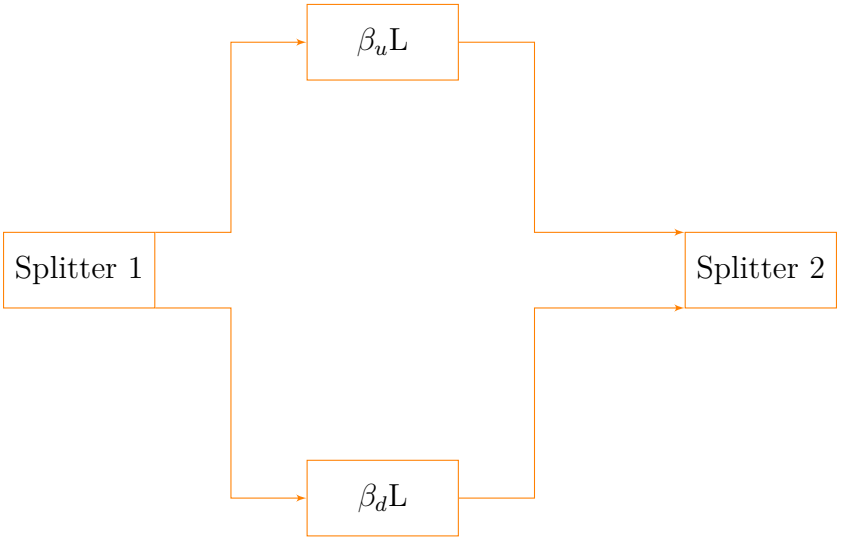

Figure 4: Schematic of MZI

$$T_{MZI_f} = T^T_{MZI_b} = \sqrt{\gamma_1}\sqrt{\gamma_2}\begin{pmatrix} t_1 & k_1^* \\ -k_1 & t_1^* \end{pmatrix} \cdot \begin{pmatrix} e^{(\alpha+j\beta_d)L} & 0 \\ 0 & e^{(\alpha+j\beta_u)L} \end{pmatrix} \cdot \begin{pmatrix} t_2 & k_2^* \\ -k_2 & t_2^* \end{pmatrix} =$$

$$\sqrt{\gamma_1}\sqrt{\gamma_2}\begin{pmatrix} t_1 e^{(\alpha j\beta_u)L} t_2 - k_1^* e^{(\alpha j\beta_d)L} k_2 & +k_1^* e^{(\alpha+j\beta_d)L} t_2^* + t_1 e^{(\alpha+j\beta_u)L} k_2^* \\ -k_1 e^{(\alpha+j\beta_u)L} t_2 - t_1^* e^{(\alpha+j\beta_d)L} k_2 & t_1^* e^{(\alpha-j\beta_d)L} t_2^* - k_1 e^{(\alpha+j\beta_u)L} k_2^* \end{pmatrix} \tag{17}$$

Depending on the splitters used it is possible to distinguish between three cases:

1. Both splitters of 2 outputs and inputs.
2. One splitter of 1 input and 2 outputs and the other of 2 inputs and 2 outputs.
3. One splitter of 1 input and 2 outputs and the other of 2 inputs and 1 output.

This work explores the first two options because it allows to build a reflective Sagnac interferometer.

Case 1: both splitters of two inputs and two outputs

Applying the equations eqs. (12), (14) and (17) and making the simplification of eq. (18),the transfer matrix of a 2x2 MZI is:

$$\begin{cases} K_a \cong K_b \\ \alpha_u L \cong \alpha_d L \cong 0 \\ \Delta\Phi = L \cdot (\beta_u - \beta_d) \end{cases} \tag{18}$$

$$T_{MZI2x2_f} = T^T_{MZI2x2_b} =$$

$$\sqrt{\gamma_1}\sqrt{\gamma_2} \cdot e^{j\beta_d L_1}\begin{pmatrix} e^{+j\Delta\Phi} - 2Ke^{j\frac{\Delta\Phi}{2}} cos\frac{\Delta\Phi}{2} & -2j\sqrt{K(1-K)}e^{j\frac{\Delta\Phi}{2}} cos\frac{\Delta\Phi}{2} \\ -2j\sqrt{K(1-K)}e^{j\frac{\Delta\Phi}{2}} cos\frac{\Delta\Phi}{2} & 1 - 2Ke^{j\frac{\Delta\Phi}{2}} cos\frac{\Delta\Phi}{2} \end{pmatrix} \tag{19}$$

Case 2: one splitter of 1 input and 2 outputs and the other of 2 inputs and 2 outputs

Applying the eqs. (13), (14) and (17) and simplifying with eq. (20) the transfer matrix of a 2x2 MZI is:

$$\begin{cases} K_a \cong K_b \\ \alpha_u L \cong \alpha_d L \cong 0 \\ \Delta\Phi = L \cdot (\beta_u - \beta_d) \\ \nu = \frac{\Delta\Phi}{2} - \frac{\pi}{4} \end{cases} \tag{20}$$

$$T_{MZI1x2_f} = T^T_{MZI1x2_b} =$$

$$\sqrt{\gamma_1}\sqrt{\gamma_2} \cdot e^{j\beta_d L_1} \begin{pmatrix} 1 - 2ke^{j\nu}cos\nu & -2j\sqrt{K(1-K)}e^{j\nu}cos\nu \\ -2\sqrt{K(1-K)}e^{j\nu}cos\nu & -j(e^{j2\nu} - 2ke^{j\nu}cos\nu) \end{pmatrix} \tag{21}$$

4.5. Sagnac reflectors

As stated in section 1, our main target was to implement a tunable mirror in integrated photonics. In the literature exists differents types of reflectors as mirrors (based on total internal reflexion due to index contrast between two medias), bragg reflectors (based on bragg theory of periodic slits) [30-37] and Sagnac reflector (based on one splitter with the output ports interconected) [38-51]. In each type there are different ways to tune the reflectivity of the device but this work is focused in tunable Sagnac reflectors based on Mach-Zehnder interferometers. We have selected this device because does not require additional fabrication processes if compared with mirror-based devices (special metal deposition and trench) or Bragg gratings (high resolution lithography).
The basic example is 3 dB splitter with a feedback loop.

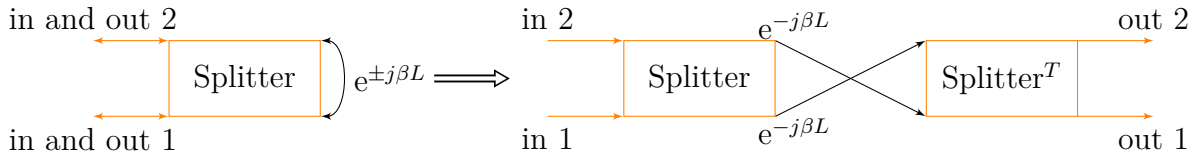

Figure 5: Schematic of a basic 2x2 Reflective Sagnac

Using formulas of eq. (16) and combining with the generic solutions of a 2 inputs and outputs splitter:

$$T_{RSL} = T_{loop} * T_{MMI} * T_{inv} * T_{MMMI_b}$$

The transfer matrix obtains the maximum when a 3dB splitter is used. To implement a tunable Reflective Sagnac a 2x2 MZI and a 1x2 MZI are used instead of splitter. Following the previous expressions eqs. (16), (19) and (21)

Case 1: RSL-2x2
Using the eqs. (16) and (19)

$$T_{RSL-2x2} = T_{loop} * T_{MZI2x2_f} * T_{inv} * T_{MZI2x2_b} \tag{22}$$

To obtain the reflection in the same port and the transmission, it is possible to operate the transmission matrix as mentioned in [15].

$$\begin{cases} r = \frac{T_{21}}{|T_{RSL-2x2}|} \\ t = \frac{T_{22}}{|T_{RSL-2x2}|} \\ R = r \cdot r^* \\ T = t \cdot t^* \end{cases} \tag{23}$$

Case 2: RSL-1x2
Using the eqs. (16) and (20)

$$T_{RSL-1x2} = T_{loop} * T_{MZI1x2_f} * T_{inv} * T_{MZI1x2_b} \tag{24}$$

Following the equations eq. (23)

$$\begin{cases} r = \frac{T_{21}}{|T_{RSL-1x2}|} \\ R = r \cdot r^* \end{cases} \tag{25}$$

These eqs. (23) and (25) give the formal solutions to be explored and compared in the next section.

5. Simulations

In this section, the behaviour of the different solutions from section 4.5 and section 4.4 and their response with the variation of the main parameters are compared. Moreover, thanks to the transfer matrices, it is easier and faster to implement any parameter change in a mathematical program as MATLAB [52].
On the other hand, to build these devices a MMI splitter was designed with updated design rules trying to obtain the best performance for splitting.

5.1. MZI vs Reflective Sagnac

The theoretical comparative between MZI and the Reflective Sagnac Loop (RSL) is made. This helps to understand the strengths and weaknesses of the reflective Sagnac interferometer.

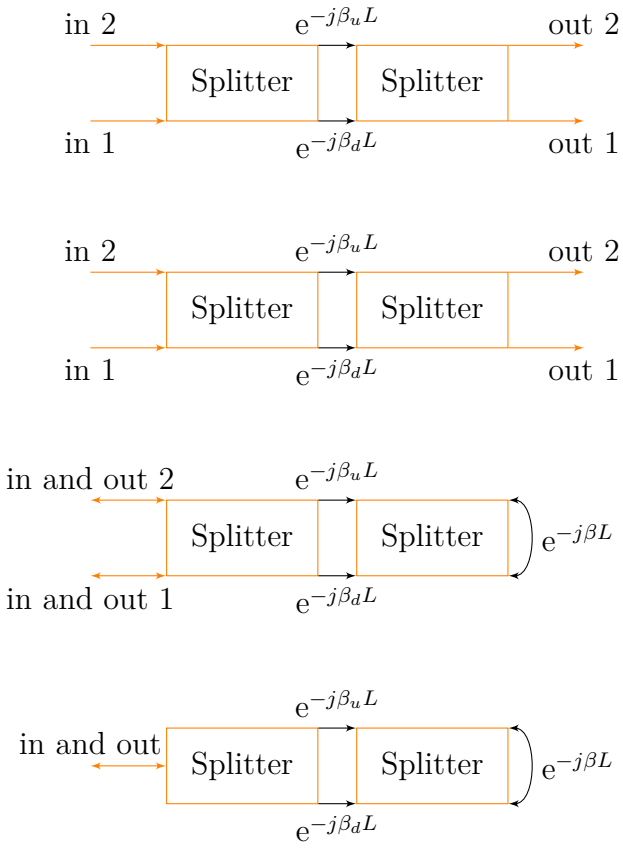

Figure 6: Schematic of 1x2 MZI, MZI2x2, Reflective Sagnac 2x2 and Reflective Sagnac 1x2

A Mach-Zehnder interferometer changes the optical output through the phase shift between arms. This phase shift achieved by introducing an extra length in one of the arms or with active dephase. There are a lot of effects that can be employed in integrated optics to obtain a phase shifter but it is possible to divide them in four categories: acoustic effect, electro-optical effect, plasma-displacement effect and thermal effect.
Acoustic, electro-optical and plasma-displacement effects need complex fabrication to control precisely the phase difference. On the other hand, the optical propagation constant can change with temperature. If higher temperature is used, more phase displacement is reached [53]. This change of the temperature could be obtained with a small electrical path on top of waveguide (heater). The resistance of a metallic material depends on their intrinsic sheet resistance (depends on the height and the material composition) and the dimensions (width and length). This heater warm up depending on the current flow applied. The disadvantages of this method is the velocity of the response, because temperature is a slow effect (milliseconds) and the power consumption, that it is too much for some applications. However this phase shifter is the best to use it in all technologies because no extra complex processes are required.
Reflective Sagnac could be simplified as two Mach-Zehnder connected. The power used

to change between maximum and minimum is called P_π. In a Reflective Sagnac this P_π is half of the P_π of a single MZI due to their configuration. The Mach-Zehnders and the Reflective Sagnac are composed of two simple elements: waveguides, phase shifters and splitter. The main characteristics of the waveguides are the propagation losses and the length.
The propagation losses of an specific geometry of waveguide depends on the material and the roughness of the side-walls of the waveguide that can introduce high scattering losses. The length of the waveguide modify the total insertion losses of the waveguide section and the phase shift. The phase shifter also introduces a phase shift but with an external active signal. The insertion losses are comparable with a waveguide with the same length. Moreover, the splitters have two main parameters: excess loss and imbalance. The imbalance is the power distribution between the outputs of the splitter. The excess loss is the extra losses introduced by the splitter due to their configuration. In the next subsections a comparative analysis is made of these parameters between MZI and Reflective Sagnac.

5.1.1. Tuning response of phase shifters: control of Amplitude and Phase

In this sub-section, the splitters will have an ideal configuration:: excess loss $\cong 0$, α L $\cong 0$ and K $\cong 0.5$. The amplitude and phase of the RSL and MZI depend on the phase difference in the phase shifters.

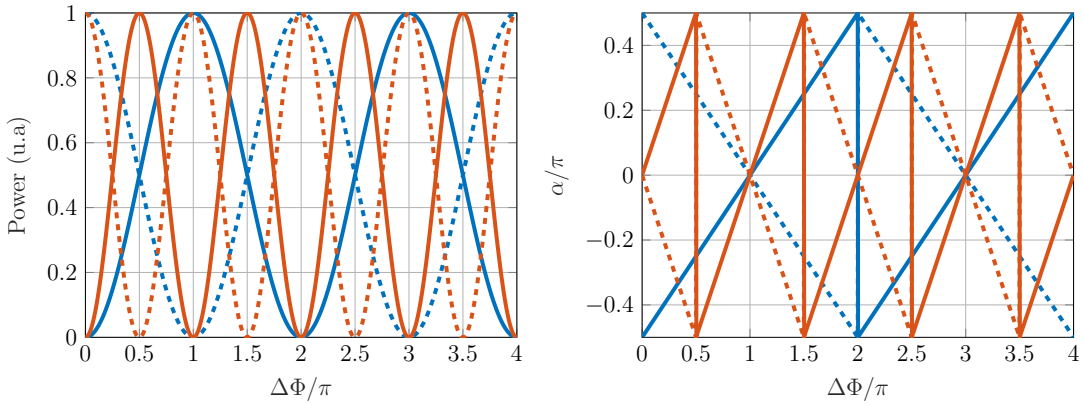

(a) Amplitude **(b)** Phase

Figure 7: Comparative figure between 2x2 MZI and RSL 2x2. Transmision of MZI in the cross-port (solid blue line), transmision of MZI in the direct-port (dots blue line), transmision of RSL (solid red line), reflection of RSL (dots red line).

The figure Section 5.1.1 shows the improvement of reflective Sagnac regarding of P_π as mentioned before.
In a passive and ideal state of symmetric Mach-Zehnder interferometer 2x2, the formulas show that when input power is launched in the 1st input all the power goes to the cross port. Tuning the phase shift difference between arms to π we can switch the power completely to the opposite output. In contrast, the 2x2 RSL in $\pi/2$ state, all power goes

to the same input waveguide. Moreover, in π state all power returns to the transmission port.

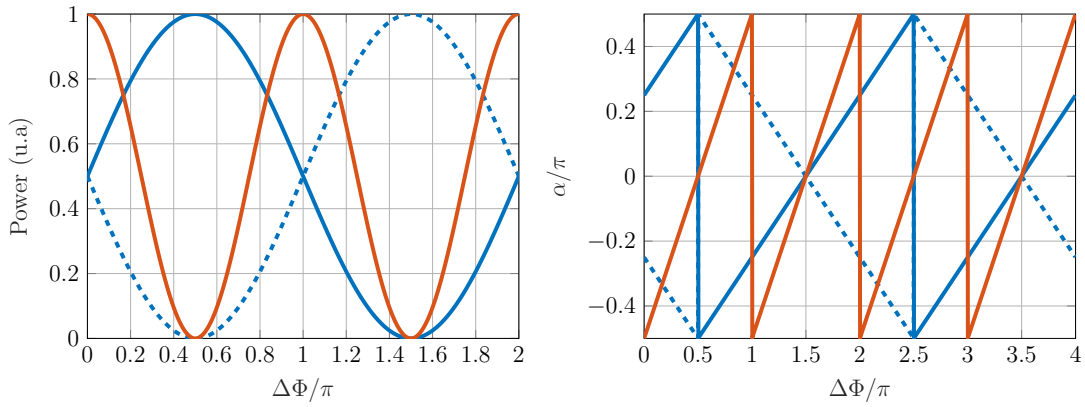

(a) Amplitude **(b)** Phase

Figure 8: Comparative figure between 1x2 MZI and RSL 1x2. Transmision of MZI in the cross-port (solid blue line), transmision of MZI in the direct-port (dots blue line), reflection of RSL (dots red line).

In a passive and ideal state of symmetric 1x2 Mach-Zehnder interferometer , the formulas shows that when input power is launched in the input port the power is divided equally between the output ports. Tuning the phase difference between arms to $\pi/2$ the power goes completely to one of the outputs. On the other hand, the 1x2 RSL in 0 phase shift, all power is reflected to the same input port and in $\pi/2$ state all power is lost to the lossy mode.
One interesting property of these devices are the control of the phase. If both phase shifters are modified at the same time, by changing the refractive index of both waveguides, the output amplitude distribution remains equal because it depends on the phase difference. However, the phase distribution of the both outputs changes with the change of both phase shifters.

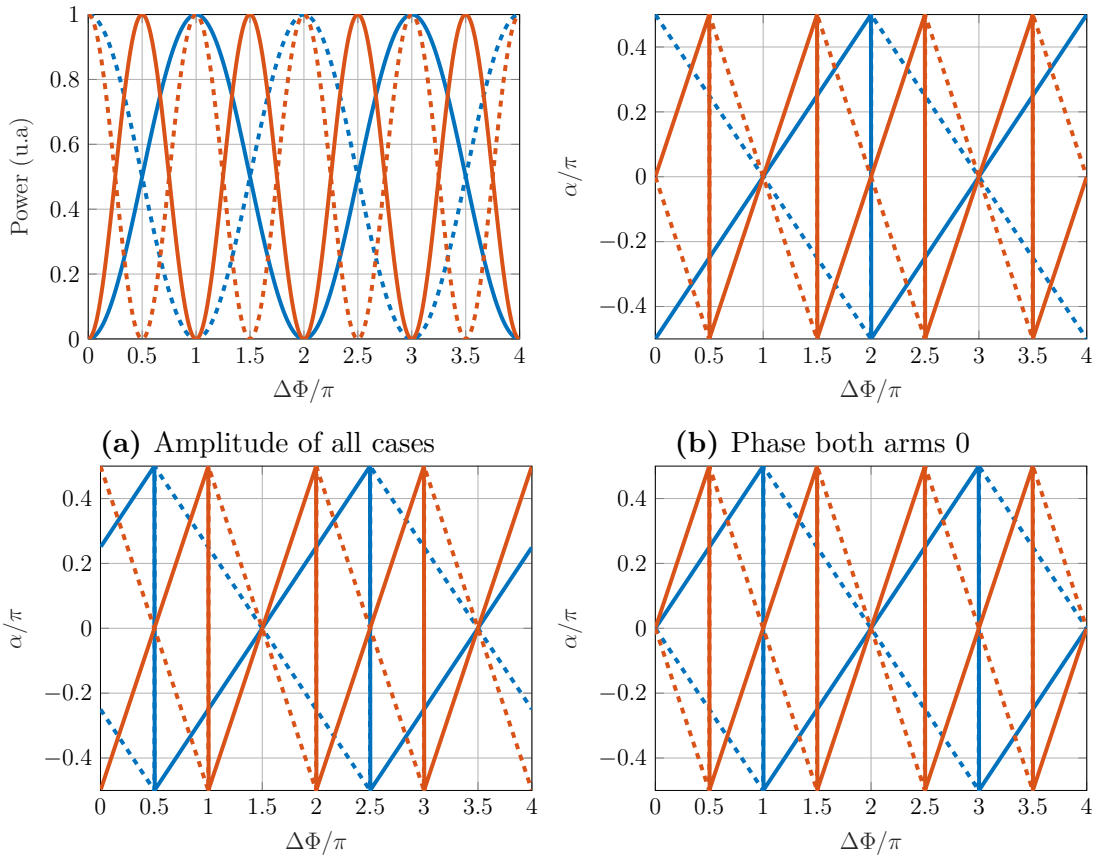

(a) Amplitude of all cases

(b) Phase both arms 0

(c) Phase both arms $\pi/4$

(d) Phase both arms $\pi/2$

Figure 9: Comparative figure between 2x2 MZI and RSL 2x2 adding phase in both arms. Transmision of MZI in the cross-port (solid blue line), transmision of MZI in the direct-port (dots blue line), transmision of RSL (solid red line), reflection of RSL (dots red line).

As shown the Fig. 9 the phase response of RSL 2x2 could be tuned by applying the same phase shift in both arms. This property is really interesting as to correct the phase relations in Arrayed Waveguide Gratings (AWGs) [29]. The change in the phase allows you to adjust individually the phase response.

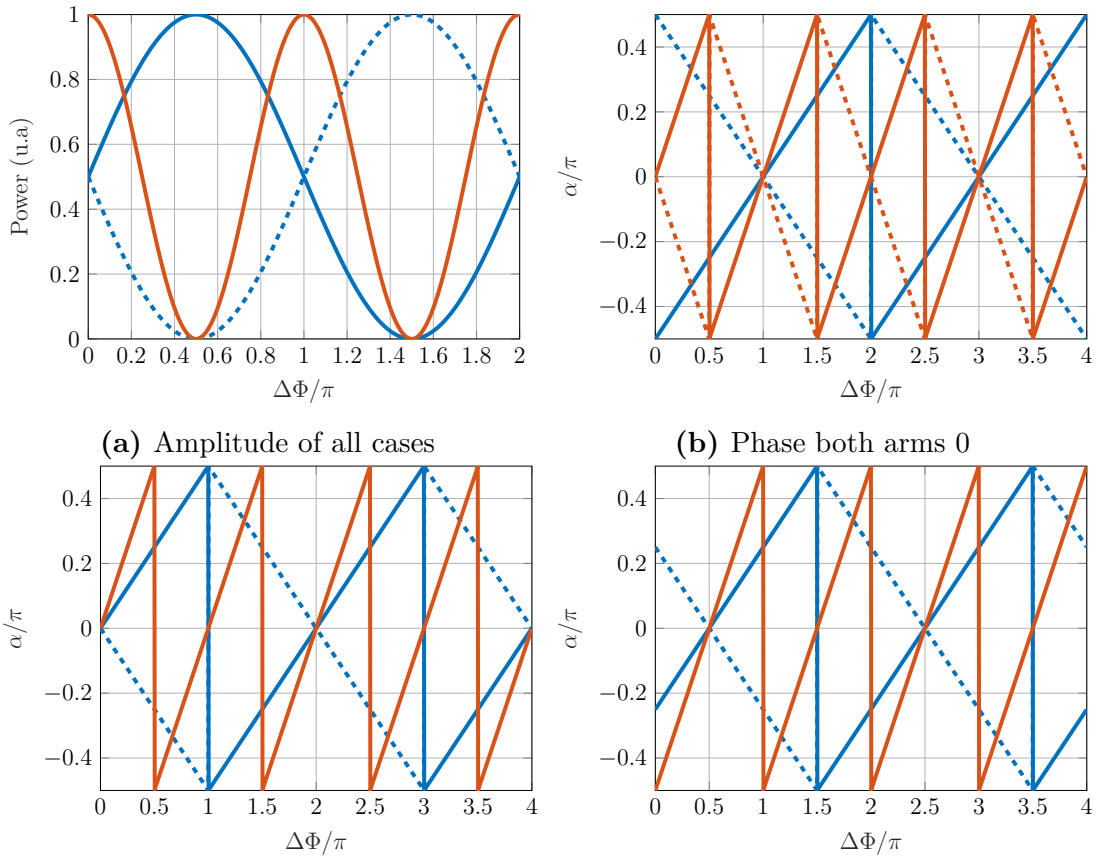

(a) Amplitude of all cases

(b) Phase both arms 0

(c) Phase both arms $\pi/4$

(d) Phase both arms $\pi/2$

Figure 10: Comparative figure between 1x2 MZI and RSL 1x2 adding phase in both arms. Transmision of MZI in the cross-port (solid blue line), transmision of MZI in the direct-port (dots blue line), reflection of RSL (solid red line).

In the 1x2 RSL all power is reflected, this change of the phase can be very useful for tuning an AWG spectral response. Also, one remarkable property is that the maximum phase shift in both arms is π. When a $\pi/4$ phase shift is reached, the phase relation of the input changes to the half of the phase.

5.1.2. Changing excess loss and propagation losses

The propagation losses of the waveguides add a real value that multiplies all the matrices. This parameter with excess losses of the splitters reduces the maximum output power. Only the amplitude is shown because the phase relation of the outputs don't change.

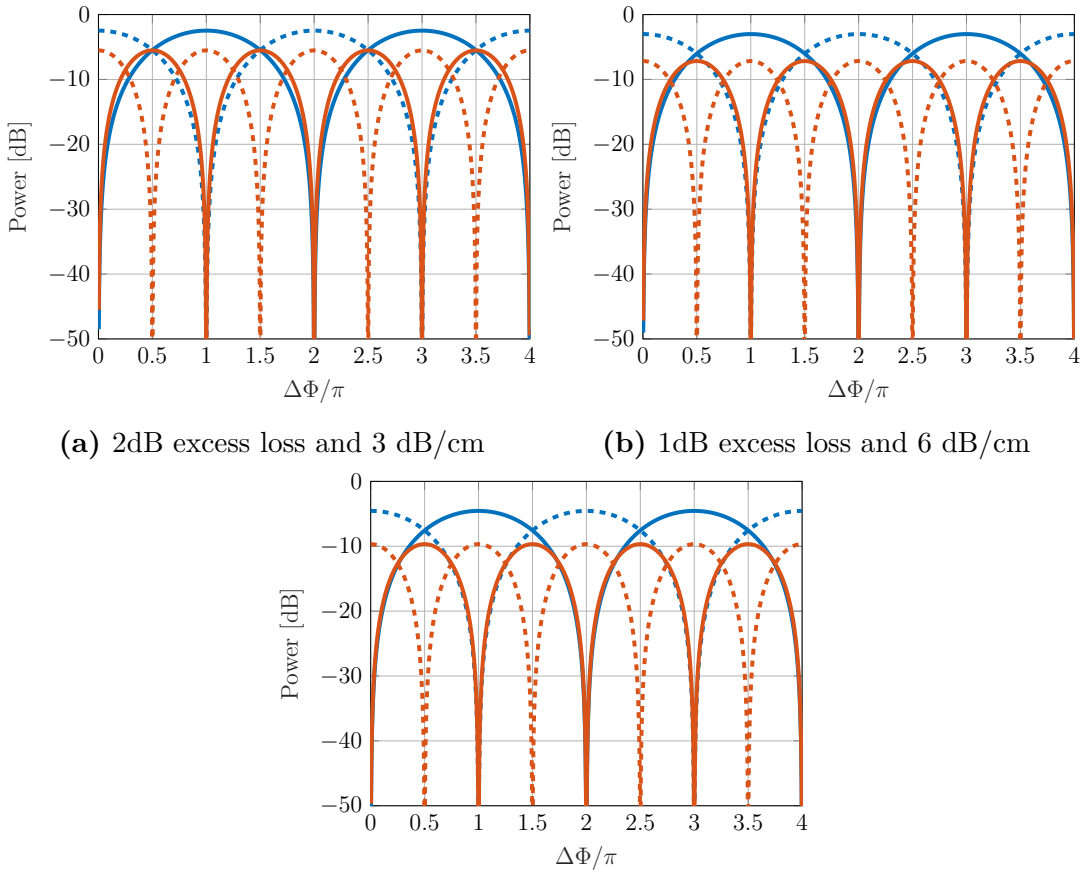

(a) 2dB excess loss and 3 dB/cm

(b) 1dB excess loss and 6 dB/cm

(c) 2dB excess loss and 3 dB/cm

Figure 11: Comparative figure between 2x2 MZI and RSL 2x2 changing excess loss and propagation losses. Transmision of MZI in the cross-port (solid blue line), transmision of MZI in the direct-port (dots blue line), transmision of RSL (solid red line), reflection of RSL (dots red line).

As shown the Fig. 11 the propagation losses don't introduce a lot of difference in the MZI and in RSL response. This is becaus the length of these devices are in the order of cents of micrometers and the propagation losses are in dB/cm. However the difference in the excess loss of the devices introduces more differences between MZI and RSL. This difference is because the RSL is like two MZI connected so, any change of excess losses in the splitters increase the difference between maximum of MZI and maximum of RSL.

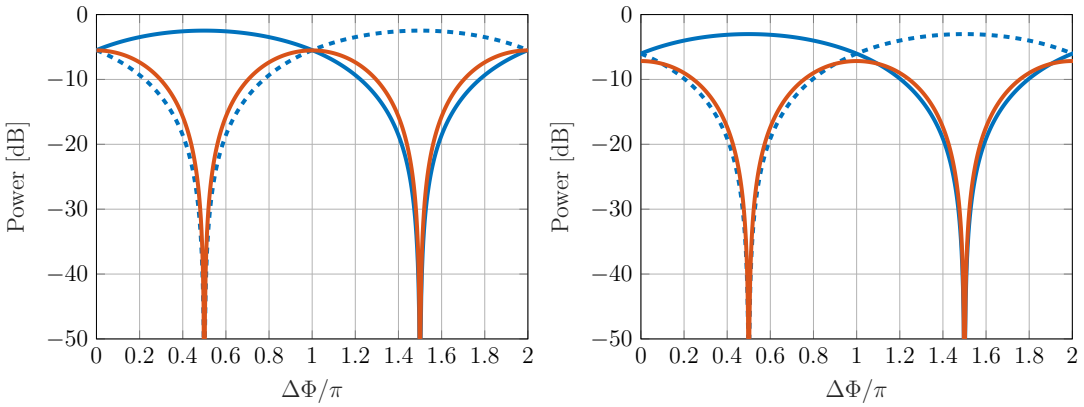

(a) 2dB excess loss and 3 dB/cm

(b) 1dB excess loss and 6 dB/cm

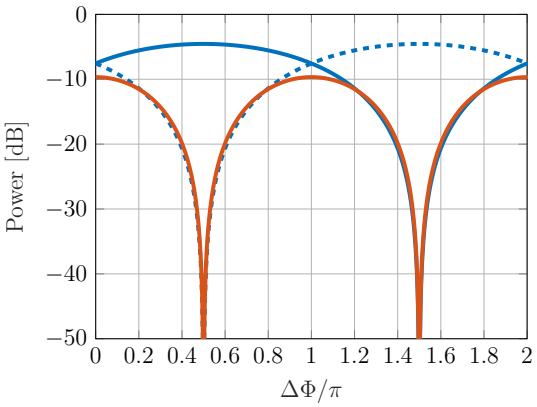

(c) 2dB excess loss and 3 dB/cm

Figure 12: Comparative figure between 1x2 MZI and RSL 1x2 changing excess loss and propagation losses. Transmision of MZI in the cross-port (solid blue line), transmision of MZI in the direct-port (dots blue line), reflection of RSL (solid red line).

As shown in Fig. 12 the behaviour is similar than in the 2x2 case. The increasing of the propagation losses doesn't change the total insertion losses a lot but the change in the excess losses increase the differences between MZI and RSL.

5.2. Splitter design

The splitter design was based on the Multimode Interference Coupler (MMI). As explained in the previous sections, these devices are quasi broadband and strong to the fabrication tolerances.
Numerical methods like Beam propagation Method (BPM) [54] can be used to simulate the optical propagation of these devices. The simulations were made with Optodesigner program [55]. This program implements BPM-1D with effective index method (EIM) [56]. First, the modes of the MMI body waveguide cross-section desired (width and height) are obtained with a mode solver. Afterwards, the L_π is obtained:

$$L_\pi = \frac{0.5 * \lambda}{n_{eff0} - n_{eff1}} \tag{26}$$

being n_{eff0} and n_{eff1} the effective refractive index of the first and second mode.
Using L_π and the width of the MMI, the theoretical formulas provide the locations of the inputs and the outputs to build the splitter desired. Futhermore, introducing wider input and output ports, the total insertion losses are reduced. To optimize the MMI a simulation with BPM is made.
At this point, it is the classic design flow for this element. However there are some extra design rules to take into account to design a MMI.

1. The input waveguides and the output waveguides should have enough gap between them to reduce the coupling effect between them. Any extra power in the other input or output port can change the splitting of the MMI.

2. Try to avoid the multimode effect or non adiabatic response of the device in the output ports. It is important to optimize the position of the outputs to reduce the non adiabatic response, showing a bouncing behaviour.

These issues are to try to reduce the total insertion losses of the device and to reach the splitting ratio near to 50 %.

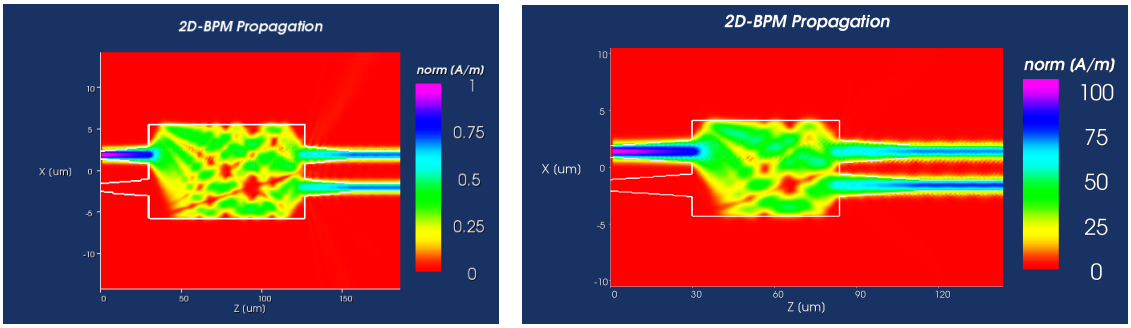

(a) Perfect align of the images **(b)** Bouncing behaviour of the output

Figure 13: Bouncing behaviour of the MMI output images

5.2.1. Material and Fabrication specifications

To corroborate the results, the fabrication of these devices was made in the Centro nacional de Microelectronica (IMB-CNM). The process was developed with the collaboration of VLC Photonics [57] and it is based on silicon nitride material.
Silicon Nitride based integration platforms are subject of attention due to the wide wavelength range over which the material is transparent (400-2400 nm) and inherently low-loss [58]. This waveguide technology is based on a combination of silicon nitride as waveguide layers, filled by and encapsulated with silica (SiO2) as cladding layers grown on a silicon wafer. SiO2 and Si3N4 layers are fabricated with CMOS-compatible industrial standard chemical vapour deposition (both low pressure, LPCVD, and plasma enhanced, PECVD)techniques, that enable cost-effective volume production [5]. The thickness is 300 nm and the monomode width for waveguides is $\cong$ 1 µm. There are processes to make metal on top for heaters, deep trenches and two levels of silicon nitride etching: 150 nm and 300 nm. These two levels allow to build two types of waveguides: deep and shallow waveguides. Deep waveguides are 300 nm thick with rectangular shape. The shallow waveguides have a slab of 150 µm thick and the waveguide is defined in the next 150 µm.
Shallow waveguides are useful because their geometry are less sensitive to the thickness variations and low loss compared with deep waveguides. However shallow waveguides are multimode and they have higher bending losses. For these last reasons the deep waveguides are better to reduce the total size of the chip and also to have monomode propagation.

Figure 14: Schematic of Deep and Shallow waveguide

5.2.2. Final designs

The designs were fabricated in a multi-project wafer run (MPW) offered by IMB-CNM [5] within a 5x5 mm^2 chip die. In this die were included designs in deep cross-section and in shallow cross-section. The most interesting is the deep cross-section devices due to the monomode behaviour. Two versions of deep MMI were designed for two inputs and two outputs. Widths of 8.4 µm and for 11.4 µm of the multimode waveguide were chosen. The narrower width is to corroborate the estimations that the coupling between arms can't be avoided and it changes the behaviour of the MMI. The design of 11 µm were designed following the rules mentioned and ideal behaviour has to be obtained.
These devices designed was introduced in MZIs and in RSL along the die to obtain the performance.

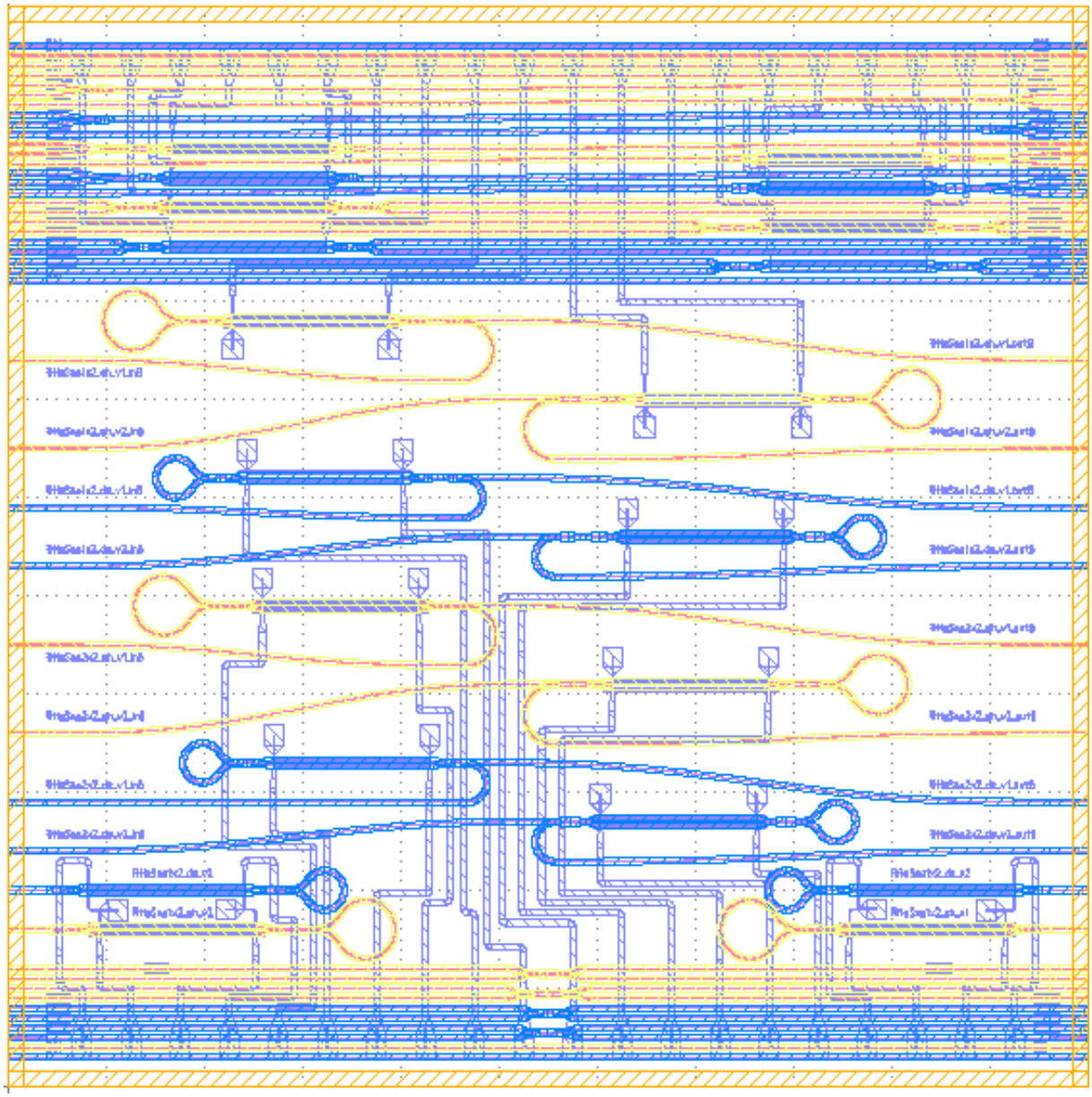

Figure 15: Die design 5.5x5.5 mm^2

6. Testing

The testing was made in the facilities of the research group [59]. An end-fire measurement setup is used with microscope objectives with MFD 2.5 µm and with polarizers, in order to inject and collect TE polarization. All structures include edge couplers at the input and at the outputs, each at one side of the chip. To measure the response an ASE broadband source was employed, together with an OSA. All the measurements are normalized to the spectrum acquired without the chip, that is between the microscope objectives face to face. All measurements are with the polarizers set to allow TE to go

through to/from the microscope objectives. Fiber collimators are employed, so as to allow fiber connections from the ASE source and to the OSA.

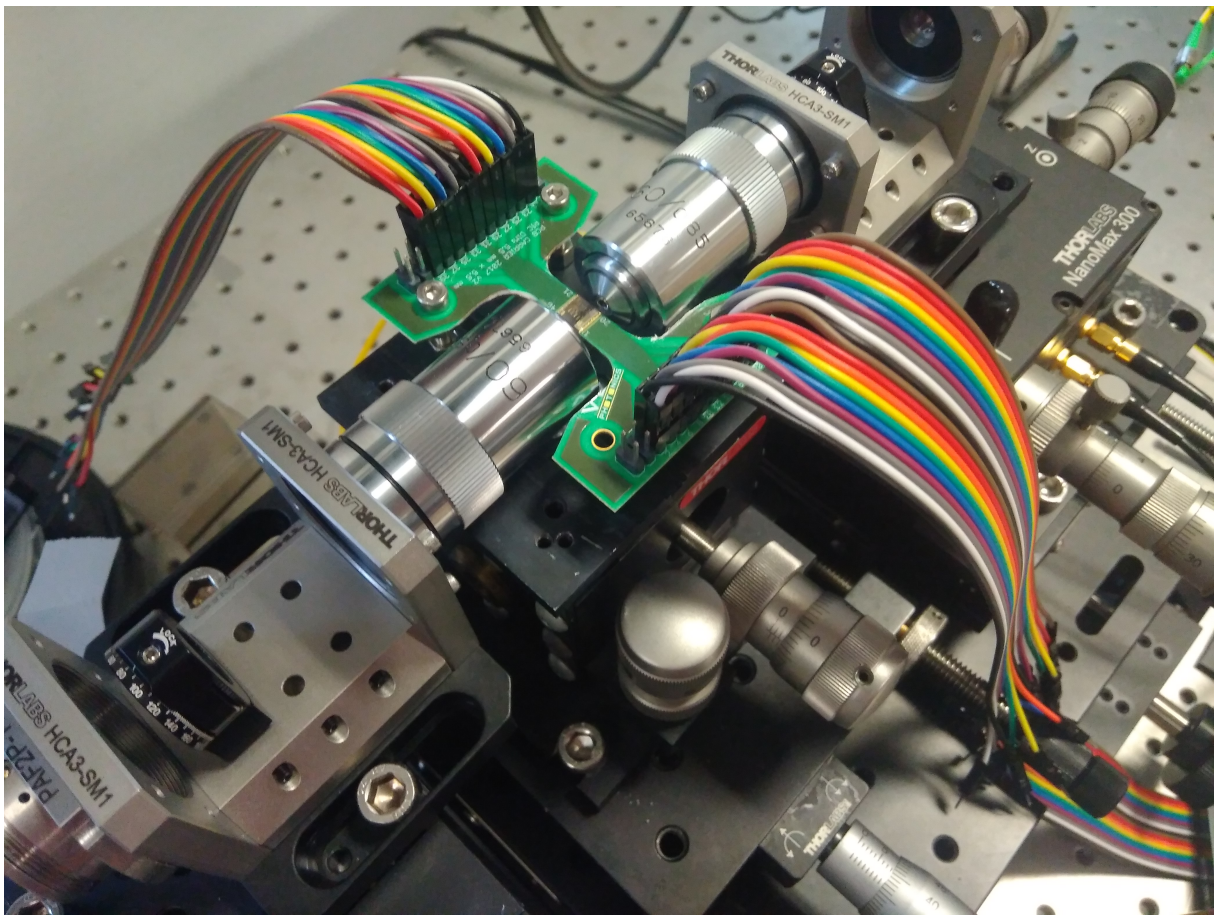

Figure 16: Setup

The wafer exposition of the full reticle of the designs allow to obtain more than one copy of the die. In the same wafer, the thicknesses are not the same along the wafer and this condition also changes the definition of the waveguides. Furthermore, the foundry provides more than one wafer so there are a lot of dies to test the variability of a specific device. The next section will study the measurements of a single die but more measurements are shown in appendix A.

6.1. Passive Measurements

The passive elements under test in this section are the 1x2 MMI and 2x2 MMI. To normalize the response and to avoid the facets response a straight waveguide is measured of the same die. The normalized power of the device under revision is obtained subtracting the power of the straight waveguide from the device power spectrum.

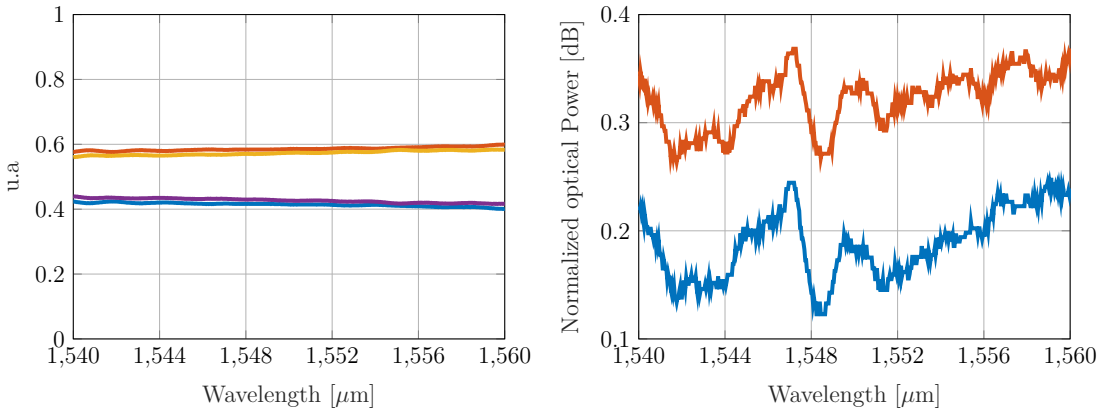

(a) Splitting ratio **(b)** Excess Loss

Figure 17: Measurements normalized of the output distribution of 2x2 MMI of 8.4 µm width.

As shown in the measurements, the behaviour is more or less stable around 60/40 splitting ratio along the different dies in the different wafers. The splitting ratio doesn't change in 20 nm bandwidth and it is flat in the full bandwidth. These devices are robust to the fabrication variations as height or width (see appendix A). The splitting ratio is not the same to the simulations (roughly 50/50). This shift in the splitting ratio can be explained because the optical inputs and outputs are coupling between them and the non ideal behaviour of the multimode sections. Regarding the excess losses, with this method is difficult to assure a good estimation because they depend on the alignment of the waveguide and the facet state in the die.

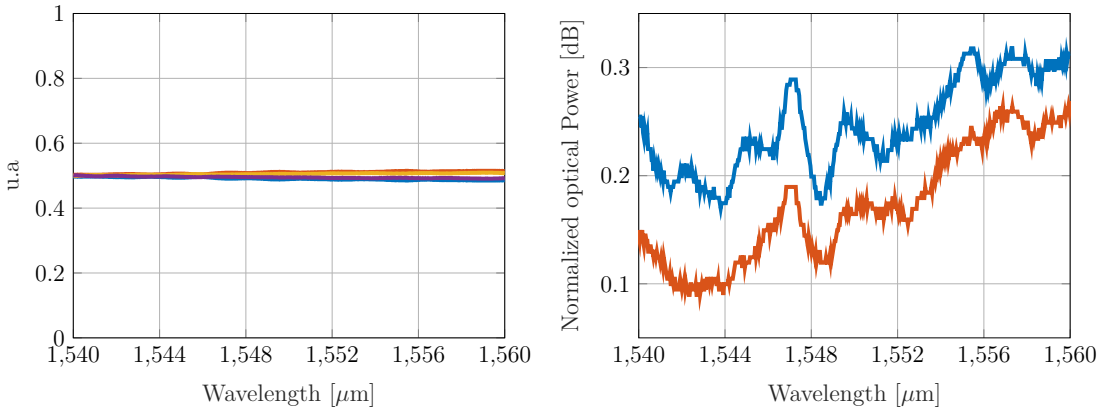

(a) Splitting ratio **(b)** Excess Loss

Figure 18: Measurements normalized of the output distribution of 2x2 MMI of 11.4 µm width.

As shown in the last figure the splitting in this version remains better in all cases in all dies (see appendix A). This fits with the concerns mentioned before because this

device has lower bouncing in the simulations, giving the idea that the output port is near to have adiabatic behaviour. The excess losses are similar to the small version. The extra losses can be explained due to the reflections inside the MMI [60]. This design is not optimized to reduce the insertion losses and the reflections. This is really important to the reflection behaviour of complex structures because these reflections sums with the total reflections. The splitting oscillates less than 5 %, ideal for high extinction ratios in the interferometers.

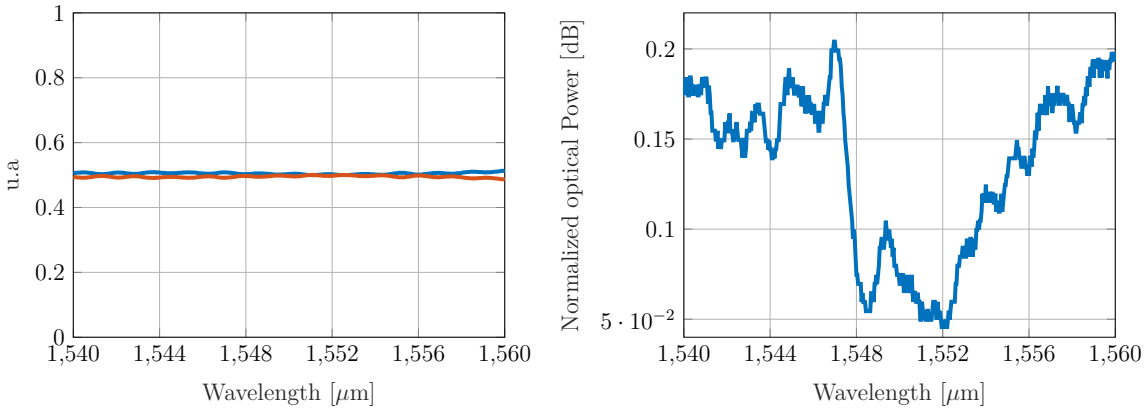

(a) Splitting ratio **(b)** Excess Loss

Figure 19: Measurements normalized of the output distribution of 1x2 MMI of 8.4 µm width.

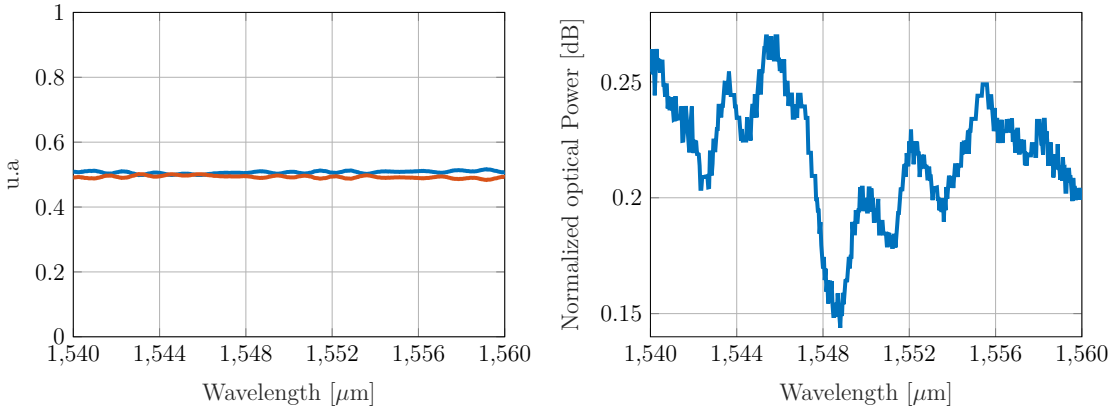

(a) Splitting ratio **(b)** Excess loss

Figure 20: Measurements normalized of the output distribution of 1x2 MMI of 11.4 µm width.

As shown in Fig. 20 the splitting is quite similar because these devices are more efficient and less sensitive to the width and thickness variations. However the power distribution shows that they have more reflections inside the MMI because they have interferometric

response (wavelength dependent response). The excess losses are lower than 2x2 MMI than can be explained because less transitions are made to reach the splitting.

6.2. Active Measurements

The active measurements were carried out using electrical probes and electrical source to the electrical contacts inside the chip. Some of the chips were glued to a PCB board to use wire bonding, making easy the connection to the chip using standard connectors.

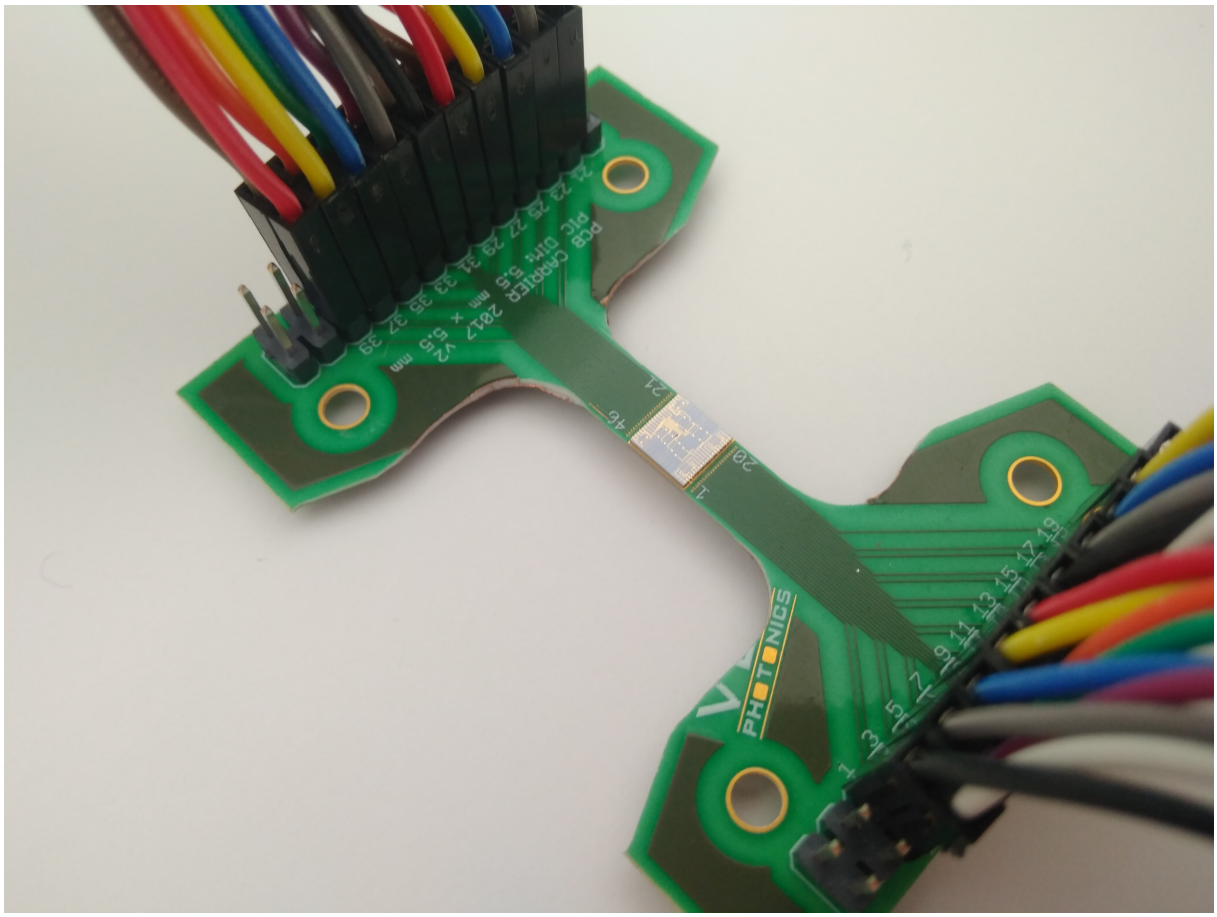

Figure 21: Photonic integration Chip on PCB

The measurements of the active elements follow the next steps:

1. Contact the electrical probes to the pads inside the chip.
2. Align the optical ports to obtain the maximum spectra.
3. Vary the electrical source.

The figures of the devices designed are:

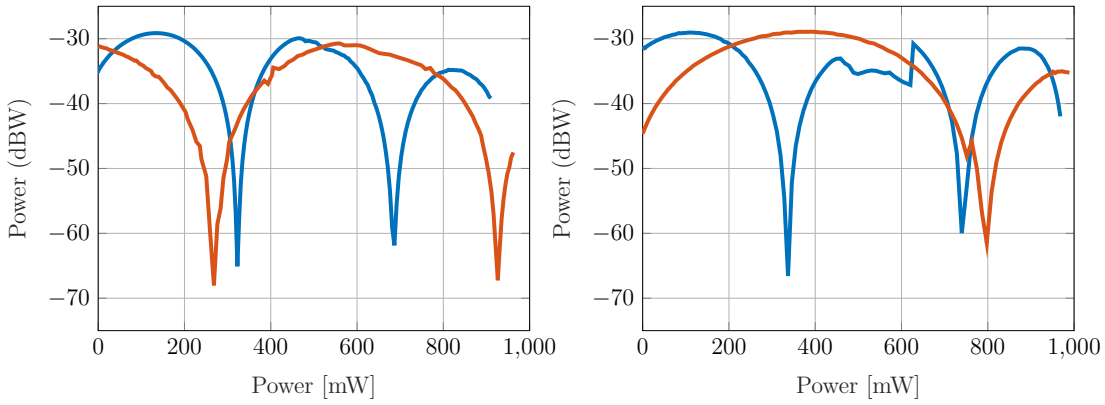

(a) Splitters of 8.4 µm width. Transmision RSL (blue), Cross-port (red)

(b) Splitters of 11.4 µm width. Transmision RSL (blue), Direct-port (red)

Figure 22: MZI versus RSL with 2x2 MMI.

As shown the Mach-Zehnder reaches one peak meanwhile the RSL reaches two peaks. This is pretty similar to the theoretical estimations and also corroborate that the K near to 50 % could reach higher extinction ratios when a pi shift is applied. On the other hand, the measurements were strongly influenced by a thermal misalignment effect. From the experiments we can derive that the physical misalignment was only in the height position. Reviewing the literature, this misalignment is produced by a mechanical variation of the stress due to the temperature of the chip [61-68]. This issue is related to the material composition of the layer stack and their expansion and compression factors depending on the temperature.
The measurements of the RSL 1x2 are strongly influenced by the thermal effect and better measurements can't be obtained. Also, they are influenced by the reflections of the elements that they hide the real response of the device.

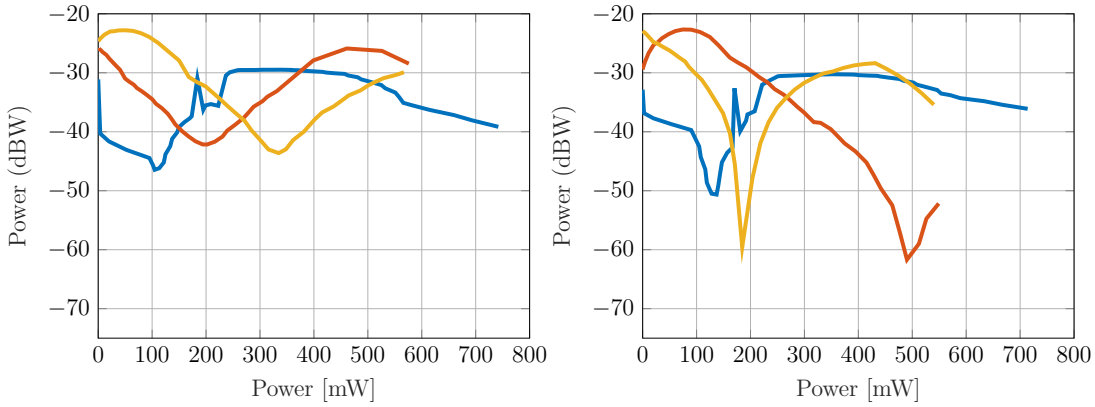

(a) Splitters of 8.4 µm width. RSL Reflection (blue), MZI Cross-port (red) and MZI Direct-port (yellow)

(b) Splitters of 11.4 µm width. RSL Reflection (blue), MZI Cross-port (red) and MZI Direct-port (yellow)

Figure 23: MZI versus RSL with 1x2 MMI.

The measurements corroborate the theorethical results developed and also show the improvement in the phase shift efficiency as a tunable reflector (see appendix A for more measurements results).

7. Conclusions and Future work

A tunable reflector was described, studied, designed and tested, corroborating the analysis made. The multimode interferometers splitter made following the new design flow described helps to obtain a quasi-perfect splitting ratio and fabrication tolerant. However, due to the reflections of the MMI, some wavelength dependent behaviour was obtained. Furthermore, a temperature expansion of the photonic chip was measured that produces an optical missalignment.
As a future work we foresee: improve the reflections of the multimode interferometer to reduce the wavelength response, try to use some methods proved in the literature to reduce the thermal expansion of the chip and the final goal is to include these structures in other bigger devices as array waveguide grating to tune the response.

8. Acknowledgments

The author acknowledge financial support through projects TEC2015-69787-REDT PIC4TB, TEC2016-80385-P SINXPECT, TEC2014-54449-C3-1-R, EC H2020-ICT-27-2015 PICs4all CSA 68777 and trough the UPV Spin-off, VLC Photonics.

9. Bibliography

[1] E. a. J. Marcatili. "Dielectric Rectangular Waveguide and Directional Coupler for Integrated Optics". En: *Bell System Technical Journal* 48.7 (1 de sep. de 1969), págs. 2071-2102. ISSN: 1538-7305. DOI: 10.1002/j.1538-7305.1969.tb01166.x. URL: https://onlinelibrary.wiley.com/doi/abs/10.1002/j.1538-7305.1969.tb01166.x (visitado 14-08-2018).

[2] S. E. Miller. "Integrated optics: An introduction". En: *The Bell System Technical Journal* 48.7 (sep. de 1969), págs. 2059-2069. ISSN: 0005-8580. DOI: 10.1002/j.1538-7305.1969.tb01165.x.

[3] Bernardo Gargallo y col. "Reflective arrayed waveguide gratings based on Sagnac loop reflectors with custom spectral response". En: *Optics Express* 22.12 (16 de jun. de 2014), págs. 14348-14362. ISSN: 1094-4087. DOI: 10.1364/OE.22.014348. URL: https://www.osapublishing.org/oe/abstract.cfm?uri=oe-22-12-14348 (visitado 09-09-2018).

[4] H. Takahashi, S. Suzuki e I. Nishi. "Wavelength multiplexer based on SiO/sub 2/-Ta/sub 2/O/sub 5/ arrayed-waveguide grating". En: *Journal of Lightwave Technology* 12.6 (jun. de 1994), págs. 989-995. ISSN: 0733-8724. DOI: 10.1109/50.296189.

[5] *Silicon Nitride Technology.* URL: http://www.imb-cnm.csic.es/index.php/en/clean-room/silicon-nitride-technology (visitado 02-09-2018).

[6] X. J. Leijtens y M. K. Smit. "S-matrix-oriented CAD tool for photonic integrated circuits. In Integrated Optic Devices II". En: *SPIE International Society for Optics and Photonics* 3278 (1998), págs. 6-13.

[7] C. Bachiller y col. "Efficient Technique for the Cascade Connection of Multiple Two-Port Scattering Matrices". En: *IEEE Transactions on Microwave Theory and Techniques* 55.9 (sep. de 2007), págs. 1880-1886. ISSN: 0018-9480. DOI: 10.1109/TMTT.2007.904076. URL: http://ieeexplore.ieee.org/document/4298198/ (visitado 15-08-2018).

[8] Joseph W. Goodman y Lam. Jane C. "Fan in loss in electrical and optical circuits and systems." En: *First International Workshop on Massively Parallel Processing Using Optical Interconnections. IEEE* 0 (1994), págs. 159-168.

[9] R. B. . Balili. "Transfer matrix method in nanophotonics". En: *In International Journal of Modern Physics: Conference Series* 17 (2012), págs. 159-168.

[10] I. Anderson. "Transmission performance of Y-junctions in planar dielectric waveguide". En: *IEE Journal on Microwaves, Optics and Acoustics* 2.1 (ene. de 1978), págs. 7-. ISSN: 0308-6976. DOI: 10.1049/ij-moa.1978.0002.

[11] W. Burns y A. Milton. "An analytic solution for mode coupling in optical waveguide branches". En: *IEEE Journal of Quantum Electronics* 16.4 (abr. de 1980), págs. 446-454. ISSN: 0018-9197. DOI: 10.1109/JQE.1980.1070501.

[12] R. H. Rediker y F. J. Leonbercer. "Analysis of Integrated-Optics Near 3 dB Coupler and Mach-Zehnder Interferometric Modulator Using Four-Port Scattering Matrix". En: *IEEE Transactions on Microwave Theory and Techniques* 30.10 (oct. de 1982), págs. 1801-1804. ISSN: 0018-9480. DOI: 10.1109/TMTT.1982.1131324.

[13] Masayuki Izutsu, Yoshiharu Nakai y Tadasi Sueta. "Operation mechanism of the single-mode optical-waveguide Y junction". En: *Optics Letters* 7.3 (1 de mar. de 1982), pág. 136. ISSN: 0146-9592, 1539-4794. DOI: 10.1364/OL.7.000136. URL: https://www.osapublishing.org/abstract.cfm?URI=ol-7-3-136 (visitado 14-08-2018).

[14] M. Kuznetsov. "Radiation loss in dielectric waveguide Y-branch structures". En: *Journal of Lightwave Technology* 3.3 (jun. de 1985), págs. 674-677. ISSN: 0733-8724. DOI: 10.1109/JLT.1985.1074216.

[15] J. Capmany y M.A. Muriel. "A new transfer matrix formalism for the analysis of fiber ring resonators: compound coupled structures for FDMA demultiplexing". En: *Journal of Lightwave Technology* 8.12 (dic. de 1990), págs. 1904-1919. ISSN: 07338724. DOI: 10.1109/50.62888. URL: http://ieeexplore.ieee.org/document/62888/ (visitado 15-08-2018).

[16] Daoxin Dai. "Advanced Passive Silicon Photonic Devices With Asymmetric Waveguide". En: *Proceedings of the IEEE* (2018), págs. 1-27. ISSN: 0018-9219, 1558-2256. DOI: 10.1109/JPROC.2018.2822787. URL: https://ieeexplore.ieee.org/document/8368063/ (visitado 17-08-2018).

[17] L. B. Soldano y E. C Pennings. "Optical multi-mode interference devices based on self-imaging: principles and applications". En: *IEEE Journal of lightwave technology* 13 (1995), págs. 615-627.

[18] M. Bachmann, P. A. Besse y H. Melchior. "General self-imaging properties in N × N multimode interference couplers including phase relations". En: *Applied Optics* 33.18 (20 de jun. de 1994), págs. 3905-3911. ISSN: 2155-3165. DOI: 10.1364/AO.33.003905. URL: https://www.osapublishing.org/ao/abstract.cfm?uri=ao-33-18-3905 (visitado 17-08-2018).

[19] R Hanfoug y col. "A Multimode Interference coupler with low reflections". En: (2005), pág. 4.

[20] A. Yariv. "Universal relations for coupling of optical power between microresonators and dielectric waveguides". En: *Electronics Letters* 36.4 (2000), pág. 321. ISSN: 00135194. DOI: 10.1049/el:20000340. URL: http://digital-library.theiet.org/content/journals/10.1049/el_20000340 (visitado 15-08-2018).

[21] Jose David Domenech Gomez. "Apodized Coupled Resonator Optical Waveguides: Theory, design and characterization". En: *Universidad Politecnica de Valencia* (2013), pág. 140.

[22] Menno Poot y col. "Design and characterization of integrated components for SiN photonic quantum circuits". En: *Optics Express* 24.7 (4 de abr. de 2016), pág. 6843. ISSN: 1094-4087. DOI: 10.1364/OE.24.006843. arXiv: 1603.01099. URL: http://arxiv.org/abs/1603.01099 (visitado 17-08-2018).

[23] Zeqin Lu y col. "Broadband silicon photonic directional coupler using asymmetric-waveguide based phase control". En: *Optics Express* 23.3 (9 de feb. de 2015), pág. 3795. ISSN: 1094-4087. DOI: 10.1364/OE.23.003795. URL: https://www.osapublishing.org/abstract.cfm?URI=oe-23-3-3795 (visitado 14-08-2018).

[24] S. Darmawan y col. "A rigorous comparative analysis of directional couplers and multimode Interferometers based on ridge waveguides". En: *IEEE Journal of Selected Topics in Quantum Electronics* 11.2 (mar. de 2005), págs. 466-475. ISSN: 1077-260X. DOI: 10.1109/JSTQE.2004.846521. URL: http://ieeexplore.ieee.org/document/1425485/ (visitado 17-08-2018).

[25] Mahmoud Tabiani y Mohsen Kavehrad. "Theory of An Efficient N x N Passive Optical Star Coupler". En: *Journal of Lightwave Technology* (2013), pág. 8.

[26] P. Munoz, D. Pastor y J. Capmany. "Modeling and design of arrayed waveguide gratings". En: *Journal of Lightwave Technology* 20.4 (abr. de 2002), págs. 661-674. ISSN: 0733-8724. DOI: 10.1109/50.996587.

[27] H. Takahashi y col. "Arrayed-waveguide grating for wavelength division multi/demultiplexer with nanometre resolution". En: *Electronics Letters* 26.2 (ene. de 1990), págs. 87-88. ISSN: 0013-5194. DOI: 10.1049/el:19900058.

[28] C. Dragone. "An N*N optical multiplexer using a planar arrangement of two star couplers". En: *IEEE Photonics Technology Letters* 3.9 (sep. de 1991), págs. 812-815. ISSN: 1041-1135. DOI: 10.1109/68.84502.

[29] M. K. Smit y C. Van Dam. "PHASAR-based WDM-devices: Principles, design and applications". En: *IEEE Journal of Selected Topics in Quantum Electronics* 2.2 (jun. de 1996), págs. 236-250. ISSN: 1077-260X. DOI: 10.1109/2944.577370.

[30] C.F.R. Mateus y col. "Ultrabroadband Mirror Using Low-Index Cladded Subwavelength Grating". En: *IEEE Photonics Technology Letters* 16.2 (feb. de 2004), págs. 518-520. ISSN: 1041-1135. DOI: 10.1109/LPT.2003.821258. URL: http://ieeexplore.ieee.org/document/1266476/ (visitado 19-08-2018).

[31] Kemiao Jia y col. "Silicon-on-insulator-based optical demultiplexer employing turning-mirror-integrated arrayed-waveguide grating". En: *IEEE Photonics Technology Letters* 17.2 (feb. de 2005), págs. 378-380. ISSN: 1041-1135. DOI: 10.1109/LPT.2004.839394.

[32] Jingwei Liu y col. "Integrated folding 4×4 optical matrix switch with total internal reflection mirrors on SOI by anisotropic chemical etching". En: *IEEE Photonics Technology Letters* 17.6 (jun. de 2005), págs. 1187-1189. ISSN: 1041-1135. DOI: 10.1109/LPT.2005.846609.

[33] E. Kleijn, M. K. Smit y X. J. M. Leijtens. "Multimode Interference Reflectors: A New Class of Components for Photonic Integrated Circuits". En: *Journal of Lightwave Technology* 31.18 (sep. de 2013), págs. 3055-3063. ISSN: 0733-8724. DOI: 10.1109/JLT.2013.2278187.

[34] L. Coldren y col. "Etched mirror and groove-coupled GaInAsP/InP laser devices for integrated optics". En: *IEEE Journal of Quantum Electronics* 18.10 (oct. de 1982), págs. 1679-1688. ISSN: 0018-9197. DOI: 10.1109/JQE.1982.1071404.

[35] R. G. DeCorby y col. "Planar omnidirectional reflectors in chalcogenide glass and polymer". En: *Optics Express* 13.16 (2005), pág. 6228. ISSN: 1094-4087. DOI: 10.1364/OPEX.13.006228. URL: https://www.osapublishing.org/oe/abstract.cfm?uri=oe-13-16-6228 (visitado 20-08-2018).

[36] A.L. Glebov y col. "Optical interconnect modules with fully integrated reflector mirrors". En: *IEEE Photonics Technology Letters* 17.7 (jul. de 2005), págs. 1540-1542. ISSN: 1041-1135. DOI: 10.1109/LPT.2005.848275. URL: http://ieeexplore.ieee.org/document/1453670/ (visitado 20-08-2018).

[37] Eric Silberstein y col. "Use of grating theories in integrated optics". En: *Journal of the Optical Society of America A* 18.11 (1 de nov. de 2001), pág. 2865. ISSN: 1084-7529, 1520-8532. DOI: 10.1364/JOSAA.18.002865. URL: https://www.osapublishing.org/abstract.cfm?URI=josaa-18-11-2865 (visitado 20-08-2018).

[38] Shan-Shan Wang y col. "All-fiber fabry–perot resonators based on microfiber Sagnac loop mirrors". En: *Optics Letters* 34.3 (1 de feb. de 2009), pág. 253. ISSN: 0146-9592, 1539-4794. DOI: 10.1364/OL.34.000253. URL: https://www.osapublishing.org/abstract.cfm?URI=ol-34-3-253 (visitado 20-08-2018).

[39] Xinhong Jiang y col. "Design and Experimental Demonstration of a Compact Silicon Photonic Interleaver Based on an Interfering Loop With Wide Spectral Range". En: *Journal of Lightwave Technology* 35.17 (1 de sep. de 2017), págs. 3765-3771. ISSN: 0733-8724, 1558-2213. DOI: 10.1109/JLT.2017.2720188. URL: http://ieeexplore.ieee.org/document/7959162/ (visitado 20-08-2018).

[40] Ting Zhang y col. "Interleaver design based on all-fiber G-T resonator formed by cascading two fiber loop mirrors". En: Photonics Asia 2004. Ed. por Hai Ming, Xuping Zhang y Maggie Yihong Chen. Beijing, China, 17 de ene. de 2005, pág. 800. DOI: 10.1117/12.570332. URL: http://proceedings.spiedigitallibrary.org/proceeding.aspx?doi=10.1117/12.570332 (visitado 20-08-2018).

[41] Jiang Xinhong y col. "Compact Silicon Photonic Interleaver Using Loop-Mirror-Based Michelson-Gires-Tournois Interferometer". En: *Optical Fiber Communication Conference*. Optical Fiber Communication Conference. Anaheim, California: OSA, 2016, Tu2F.5. ISBN: 978-1-943580-07-1. DOI: 10.1364/OFC.2016.Tu2F.5. URL: https://www.osapublishing.org/abstract.cfm?URI=OFC-2016-Tu2F.5 (visitado 20-08-2018).

[42] ITG, VDE y VDE-Verlag Gmbh. *ECOC 2016 42th European Conference on Optical Communication Proceedings, September 18 - 22, 2016, Düsseldorf, Germany*. OCLC: 959984645. 2016. ISBN: 978-3-8007-4274-5.

[43] Nan Zhou y col. "Reconfigurable and tunable compact comb filter and (de)interleaver on silicon platform". En: *Optics Express* 26.4 (19 de feb. de 2018), pág. 4358. ISSN: 1094-4087. DOI: 10.1364/OE.26.004358. URL: https://www.osapublishing.org/abstract.cfm?URI=oe-26-4-4358 (visitado 20-08-2018).

[44] Jiayang Wu y col. "Advanced photonic filters based on cascaded Sagnac loop reflector resonators in silicon-on-insulator nanowires". En: *APL Photonics* 3.4 (abr. de 2018), pág. 046102. ISSN: 2378-0967. DOI: 10.1063/1.5025833. URL: http://aip.scitation.org/doi/10.1063/1.5025833 (visitado 20-08-2018).

[45] Shuang Zheng y col. "Experimental demonstation of wavelength- and bandwidth-tunable compact integrated silicon photonic comb filter". En: *2017 Opto-Electronics and Communications Conference (OECC) and Photonics Global Conference (PGC)*. 2017 Opto-Electronics and Communications Conference (OECC) and Photonics Global Conference (PGC). Singapore: IEEE, jul. de 2017, págs. 1-3. ISBN: 978-1-5090-6293-5. DOI: 10.1109/OECC.2017.8114847. URL: http://ieeexplore.ieee.org/document/8114847/ (visitado 20-08-2018).

[46] Benedetto Troia, Francesco De Leonardis y Vittorio M.N. Passaro. "Cascaded ring resonator and Mach-Zehnder interferometer with a Sagnac loop for Vernier-effect refractive index sensing". En: *Sensors and Actuators B: Chemical* 240 (mar. de 2017), págs. 76-89. ISSN: 09254005. DOI: 10.1016/j.snb.2016.08.095. URL: http://linkinghub.elsevier.com/retrieve/pii/S0925400516313272 (visitado 20-08-2018).

[47] Jiayang Wu y col. "Integrated Fabry-Perot cavities as a mechanism for enhancing micro-ring resonator performance". En: *APL Photonics* 2.5 (mayo de 2017), pág. 056103. ISSN: 2378-0967. DOI: 10.1063/1.4981392. arXiv: 1704.07946. URL: http://arxiv.org/abs/1704.07946 (visitado 22-08-2018).

[48] Xinhong Jiang y col. "Wavelength and bandwidth-tunable silicon comb filter based on Sagnac loop mirrors with Mach-Zehnder interferometer couplers". En: *Optics Express* 24.3 (8 de feb. de 2016), pág. 2183. ISSN: 1094-4087. DOI: 10.1364/OE.24.002183. URL: https://www.osapublishing.org/abstract.cfm?URI=oe-24-3-2183 (visitado 20-08-2018).

[49] Ge Gao y col. "Tuning of resonance spacing over whole free spectral range based on Autler-Townes splitting in a single microring resonator". En: *Optics Express* 23.21 (19 de oct. de 2015), pág. 26895. ISSN: 1094-4087. DOI: 10.1364/OE.23.026895. URL: https://www.osapublishing.org/abstract.cfm?URI=oe-23-21-26895 (visitado 20-08-2018).

[50] T. A. Birks y P. Morkel. "Jones calculus analysis of single-mode fiber Sagnac reflector". En: *Applied Optics* 27.15 (1 de ago. de 1988), pág. 3107. ISSN: 0003-6935, 1539-4522. DOI: 10.1364/AO.27.003107. URL: https://www.osapublishing.org/abstract.cfm?URI=ao-27-15-3107 (visitado 20-08-2018).

[51] Junfeng Song y col. "Loop coupled resonator optical waveguides". En: *Optics Express* 22.20 (6 de oct. de 2014), pág. 24202. ISSN: 1094-4087. DOI: 10.1364/OE.22.024202. URL: https://www.osapublishing.org/abstract.cfm?URI=oe-22-20-24202 (visitado 20-08-2018).

[52] *MATLAB - El lenguaje del cálculo técnico - MATLAB & Simulink*. URL: https://es.mathworks.com/products/matlab.html (visitado 09-09-2018).

[53] Daniel Perez y col. "Thermal tuners on a Silicon Nitride platform". En: *arXiv:1604.02958 [physics]* (11 de abr. de 2016). arXiv: 1604.02958. URL: http://arxiv.org/abs/1604.02958 (visitado 01-09-2018).

[54] J. Van Roey, J. van der Donk y P. E. Lagasse. "Beam-propagation method: analysis and assessment". En: *Journal of the Optical Society of America* 71.7 (1 de jul. de 1981), pág. 803. ISSN: 0030-3941. DOI: 10.1364/JOSA.71.000803. URL: https://www.osapublishing.org/abstract.cfm?URI=josa-71-7-803 (visitado 02-09-2018).

[55] *PhoeniX Software - Solutions for micro and nano technologies*. URL: http://www.phoenixbv.com/ (visitado 02-09-2018).

[56] Mohd Haniff Ibrahim y col. "A COMBINATION APPROACH OF EFFECTIVE INDEX METHOD AND BEAM PROPAGATION METHOD IN OPTICAL DEVICE MODELLING". En: *Journal of Industrial Technology* (2008), pág. 12.

[57] *VLC Photonics Home | VLC Photonics*. URL: https://www.vlcphotonics.com/ (visitado 02-09-2018).

[58] Pascual Muñoz y col. "Silicon Nitride Photonic Integration Platforms for Visible, Near-Infrared and Mid-Infrared Applications". En: *Sensors* 17.9 (12 de sep. de 2017), pág. 2088. DOI: 10.3390/s17092088. URL: http://www.mdpi.com/1424-8220/17/9/2088 (visitado 10-09-2018).

[59] *Photonics Research Labs (PRL) – ITEAM*. URL: http://www.iteam.upv.es/group/photonics-research-labs-prl/ (visitado 03-09-2018).

[60] E. C. M. Pennings y col. "Reflection properties of multimode interference devices". En: *IEEE Photonics Technology Letters* 6.6 (jun. de 1994), págs. 715-718. ISSN: 1041-1135. DOI: 10.1109/68.300172.

[61] Jörn P Epping y col. "Ultra-low-power stress-based integrated photonic phase actuator". En: (), pág. 3.

[62] Pierre Morin y col. "A comparison of the mechanical stability of silicon nitride films deposited with various techniques". En: *Applied Surface Science* 260 (nov. de 2012), págs. 69-72. ISSN: 01694332. DOI: 10.1016/j.apsusc.2012.04.003. URL: http://linkinghub.elsevier.com/retrieve/pii/S0169433212006435 (visitado 14-08-2018).

[63] A Stoffel y col. "LPCVD against PECVD for micromechanical applications". En: *Journal of Micromechanics and Microengineering* 6.1 (1 de mar. de 1996), págs. 1-13. ISSN: 0960-1317, 1361-6439. DOI: 10.1088/0960-1317/6/1/001. URL: http://stacks.iop.org/0960-1317/6/i=1/a=001?key=crossref.2d1f7a029a4698e926ab7024fa24ff3 (visitado 14-08-2018).

[64] Martin Hubert Peter Pfeiffer y col. "Photonic Damascene Process for Low-Loss, High-Confinement Silicon Nitride Waveguides". En: *IEEE Journal of Selected Topics in Quantum Electronics* 24.4 (jul. de 2018), págs. 1-11. ISSN: 1077-260X, 1558-4542. DOI: 10.1109/JSTQE.2018.2808258. URL: https://ieeexplore.ieee.org/document/8393467/ (visitado 14-08-2018).

[65] James M Olson. "Analysis of LPCVD process conditions for the deposition of low stress silicon nitride. Part I: preliminary LPCVD experiments". En: *Materials Science in Semiconductor Processing* 5.1 (feb. de 2002), págs. 51-60. ISSN: 13698001. DOI: 10.1016/S1369-8001(02)00058-6. URL: http://linkinghub.elsevier.com/retrieve/pii/S1369800102000586 (visitado 14-08-2018).

[66] M Ghaderi, G de Graaf y R F Wolffenbuttel. "Thermal annealing of thin PECVD silicon-oxide films for airgap-based optical filters". En: *Journal of Micromechanics and Microengineering* 26.8 (1 de ago. de 2016), pág. 084009. ISSN: 0960-1317, 1361-6439. DOI: 10.1088/0960-1317/26/8/084009. URL: http://stacks.iop.org/0960-1317/26/i=8/a=084009?key=crossref.43ee132013e6fdf94d76b58461443d11 (visitado 14-08-2018).

[67] M Ghaderi, G de Graaf y R F Wolffenbuttel. "Thermal annealing of thin PECVD silicon-oxide films for airgap-based optical filters". En: *Journal of Micromechanics and Microengineering* 26.8 (1 de ago. de 2016), pág. 084009. ISSN: 0960-1317, 1361-6439. DOI: 10.1088/0960-1317/26/8/084009. URL: http://stacks.iop.org/0960-1317/26/i=8/a=084009?key=crossref.43ee132013e6fdf94d76b58461443d11 (visitado 14-08-2018).

[68] Wendian Shi y col. "MODIFYING RESIDUAL STRESS AND STRESS GRADIENT IN LPCVD SI3N4 FILM WITH ION 1MPLANTATlON". En: (), pág. 4.

A. Additional measurement results

This appendix shows other measurements for different dies for various wafers trying to see what are the imbalance response among them.
As shown in the Figs. 24 and 25 these device don't have 50/50 splitting ratio. This behaviour is predicted by the simulations because there are some coupling between the ports. The width of MMI is too small. However for the other MMI designed with the new design flow, the splitting is quasi perfect in all dies. The 1x2 MMIs have a splitting ratio near to 50 %.
The insertion losses are difficult to extract an acceptable value because it depends of the waveguide measurements, that it is the data to normalize. However, thanks to different measurements, it can be approximated that this value is less than 0.5 dB for all MMI cases.
In addition, the Figs. 32 and 33 show clearly that the 1x2 MZI and the 1x2 RSL have worse behaviour if it compares with 2x2 version. On the other hand, the graphs show that the RSL in all cases have double peaks than the MZI version.

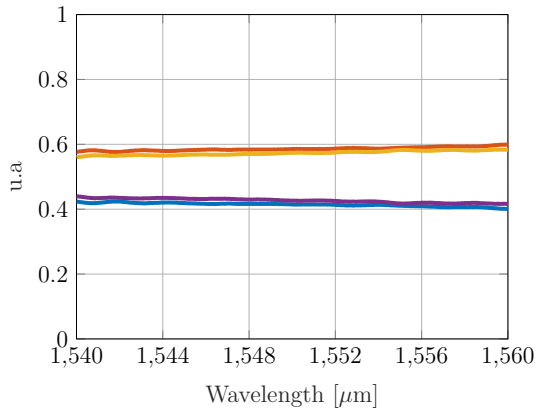

(a) Wafer 3, die 3

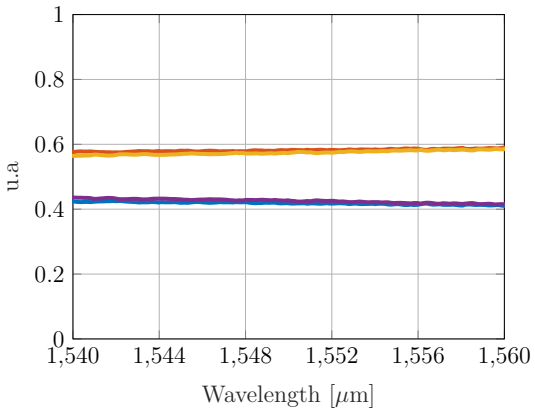

(b) Wafer 3, die 5

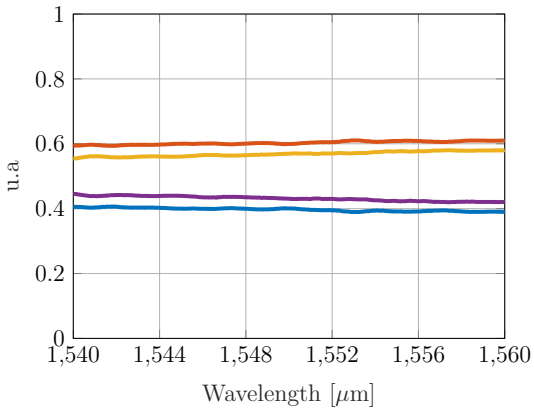

(c) Wafer 4, die 5

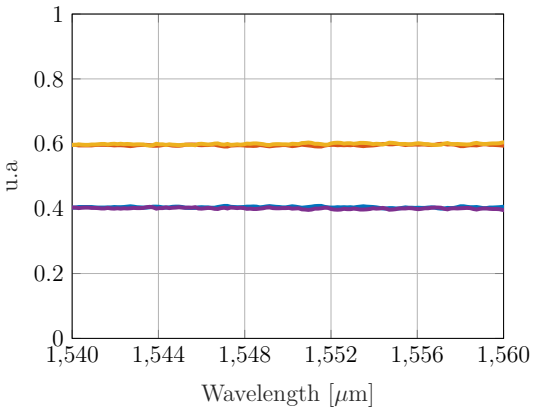

(d) Wafer 5, die 1

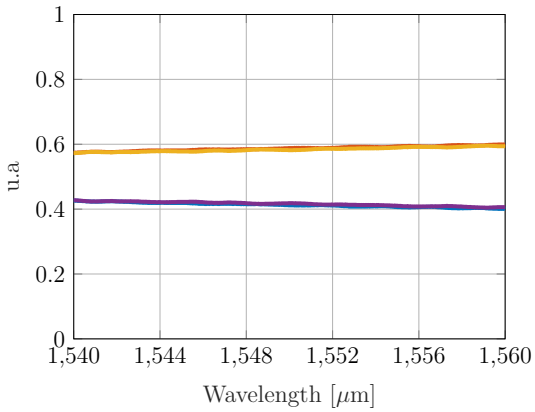

(e) Wafer 5, die 5

Figure 24: Normalized measurements the 2x2 MMI of 8.4 µm width outputs.

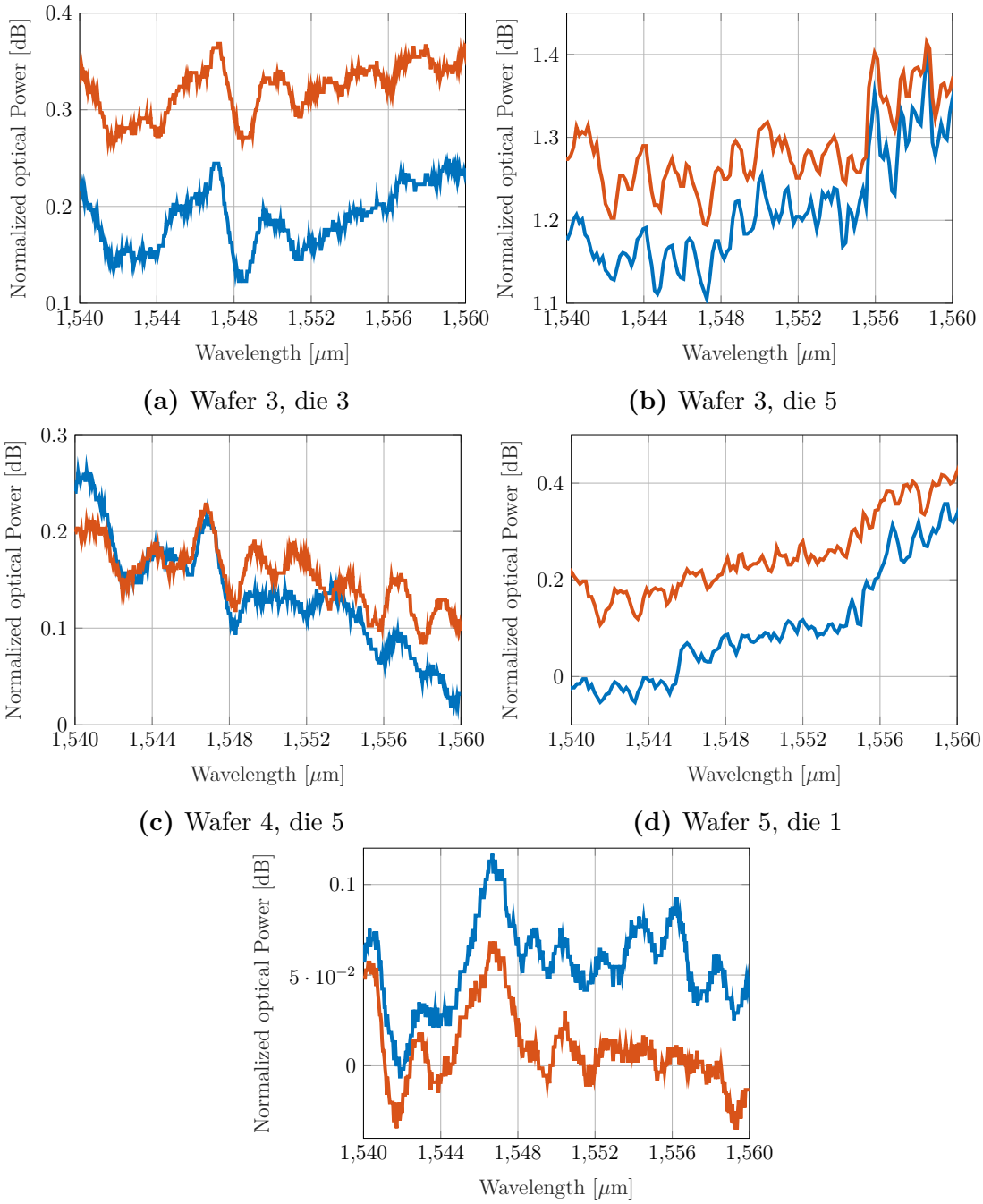

(a) Wafer 3, die 3

(b) Wafer 3, die 5

(c) Wafer 4, die 5

(d) Wafer 5, die 1

(e) Wafer 5, die 5

Figure 25: Excess losses of the 2x2 MMI of 8.4 µm width.

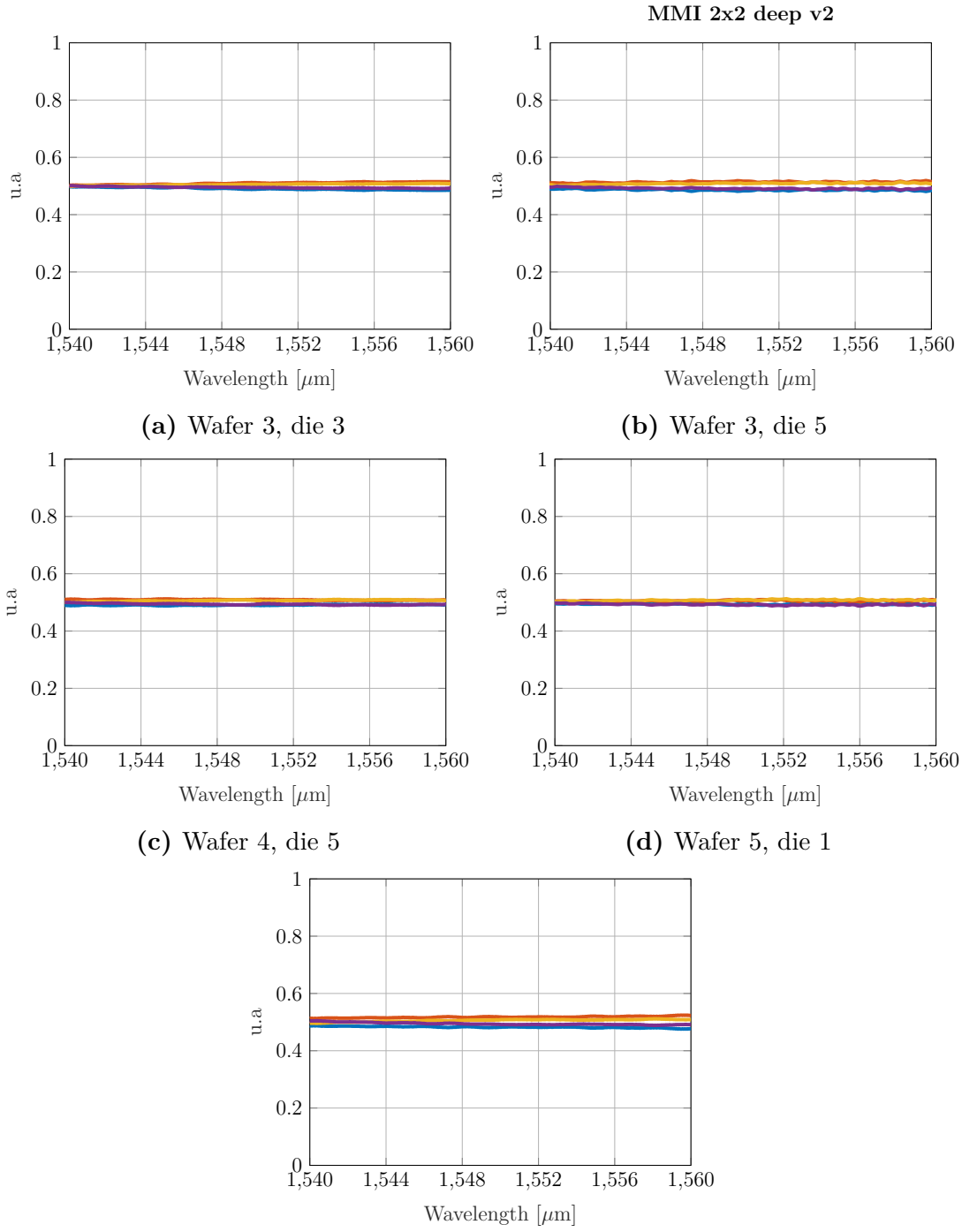

(a) Wafer 3, die 3

(b) Wafer 3, die 5

(c) Wafer 4, die 5

(d) Wafer 5, die 1

(e) Wafer 5, die 5

Figure 26: Normalized measurements the 2x2 MMI of 11.4 µm width outputs.

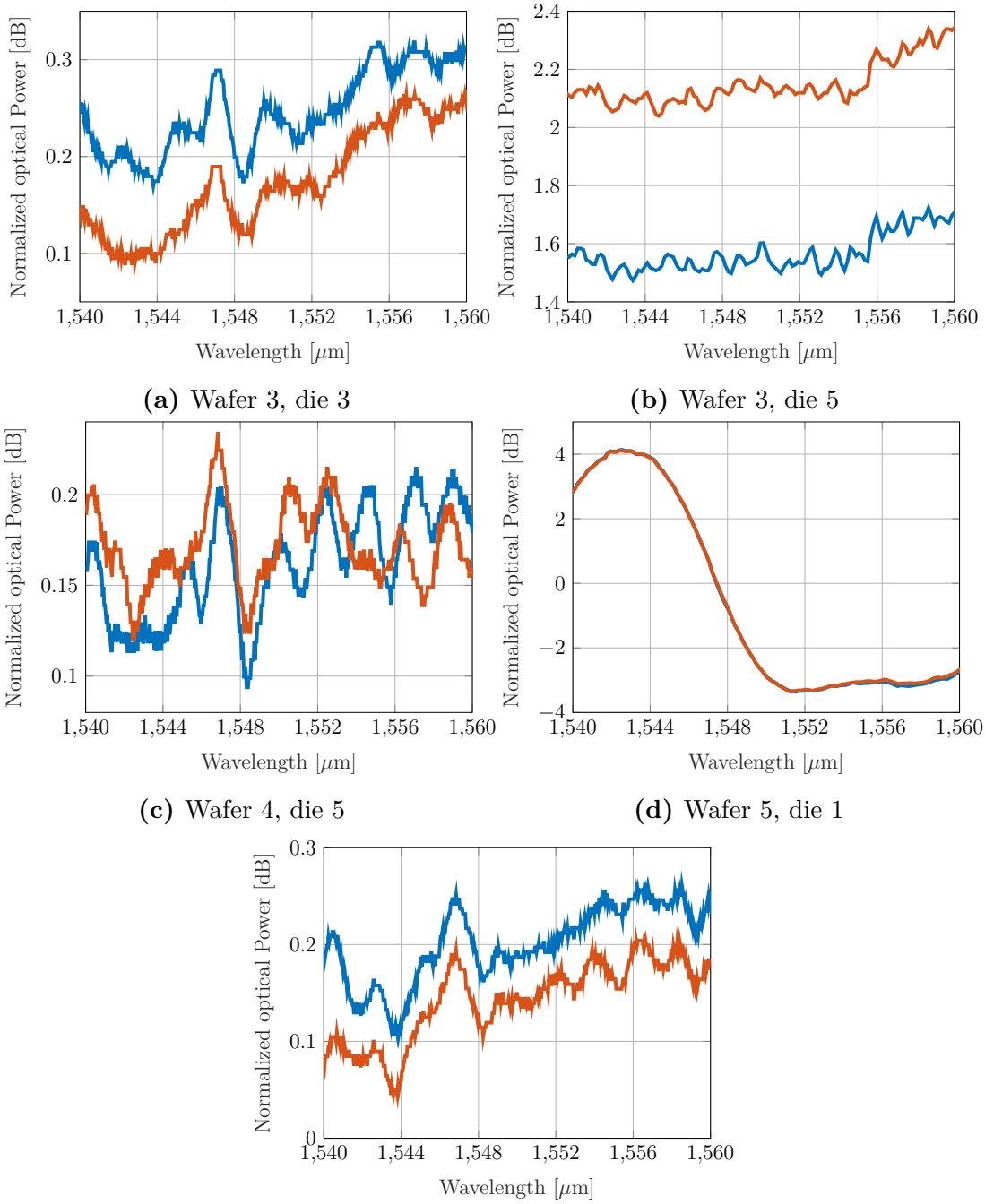

(a) Wafer 3, die 3

(b) Wafer 3, die 5

(c) Wafer 4, die 5

(d) Wafer 5, die 1

(e) Wafer 5, die 5

Figure 27: Excess losses of 2x2 MMI of 11.4 µm width.

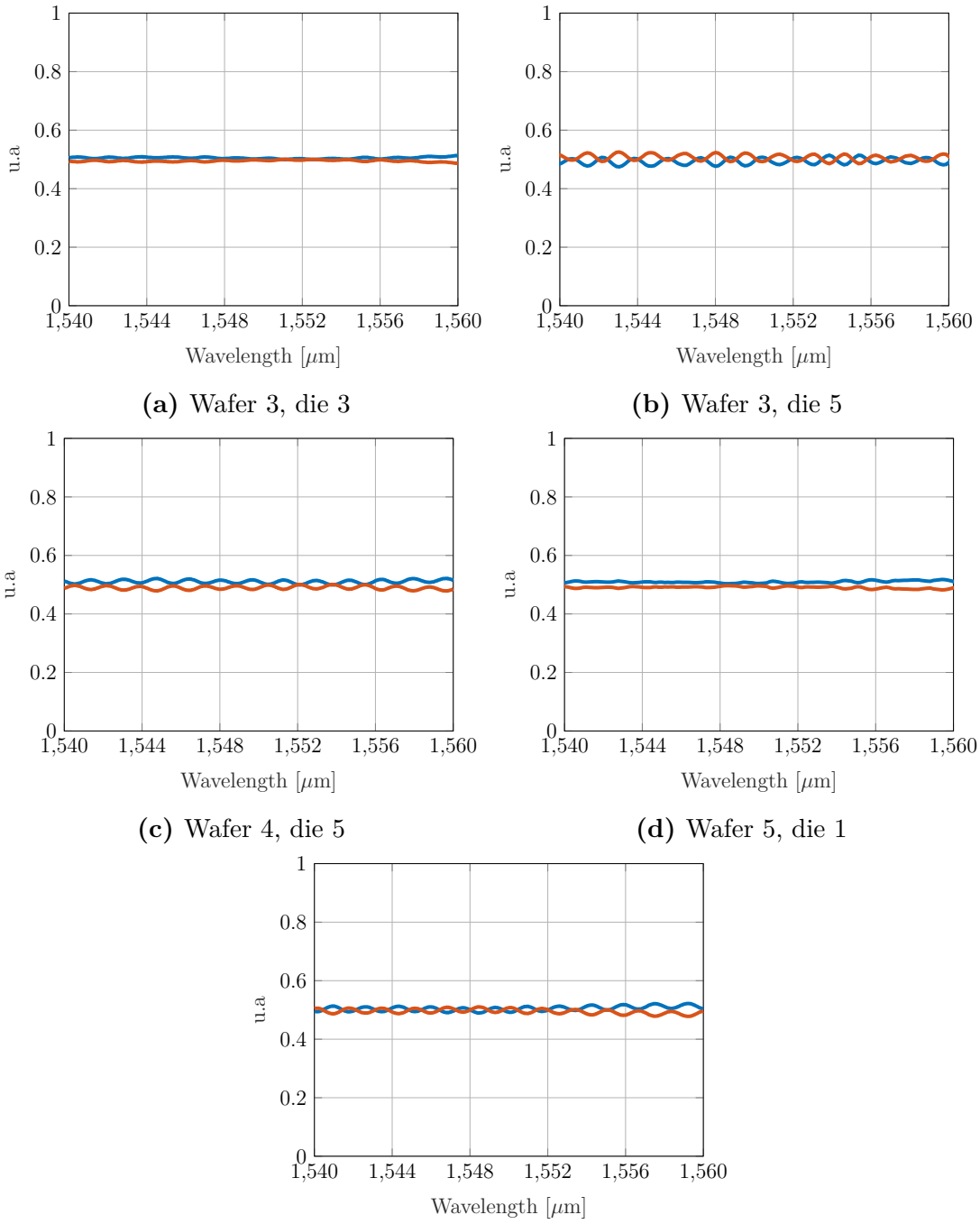

(a) Wafer 3, die 3

(b) Wafer 3, die 5

(c) Wafer 4, die 5

(d) Wafer 5, die 1

(e) Wafer 5, die 5

Figure 28: Normalized measurements the 1x2 MMI of 8.4 µm width outputs.

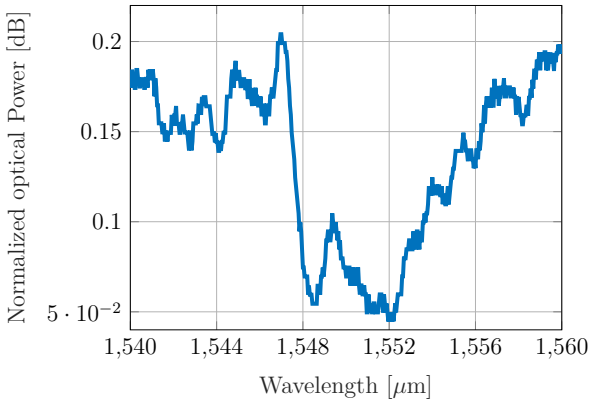

(a) Wafer 3, die 3

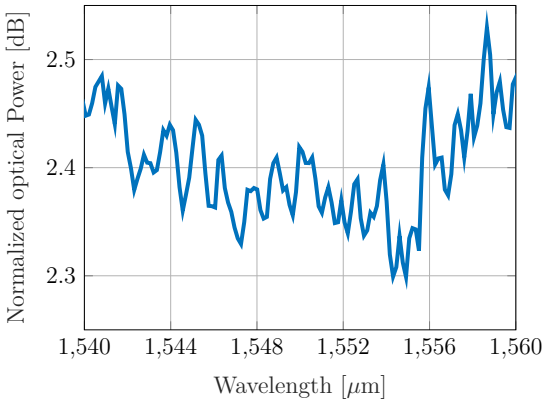

(b) Wafer 3, die 5

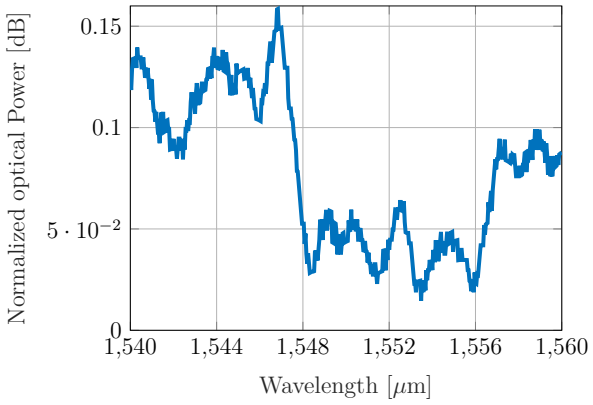

(c) Wafer 4, die 5

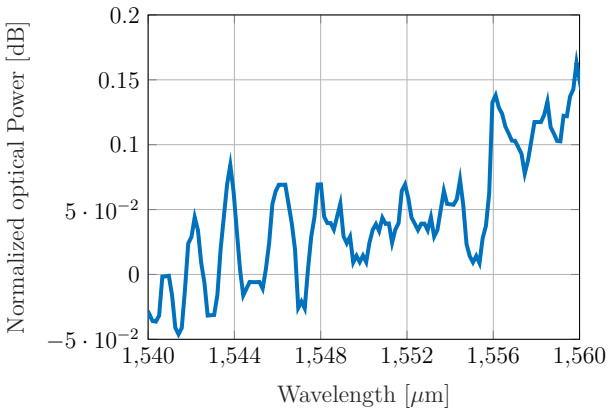

(d) Wafer 5, die 1

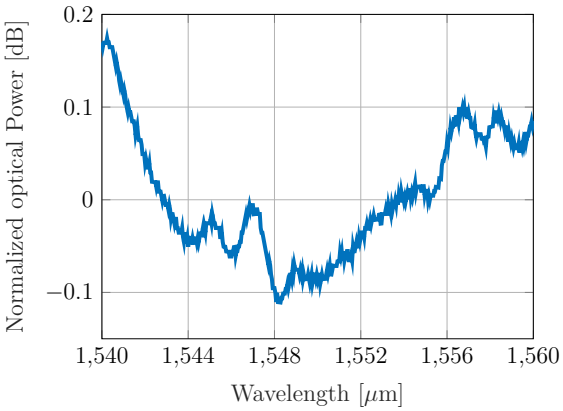

(e) Wafer 5, die 5

Figure 29: Excess losses of 1x2 MMI of 8.4 µm width.

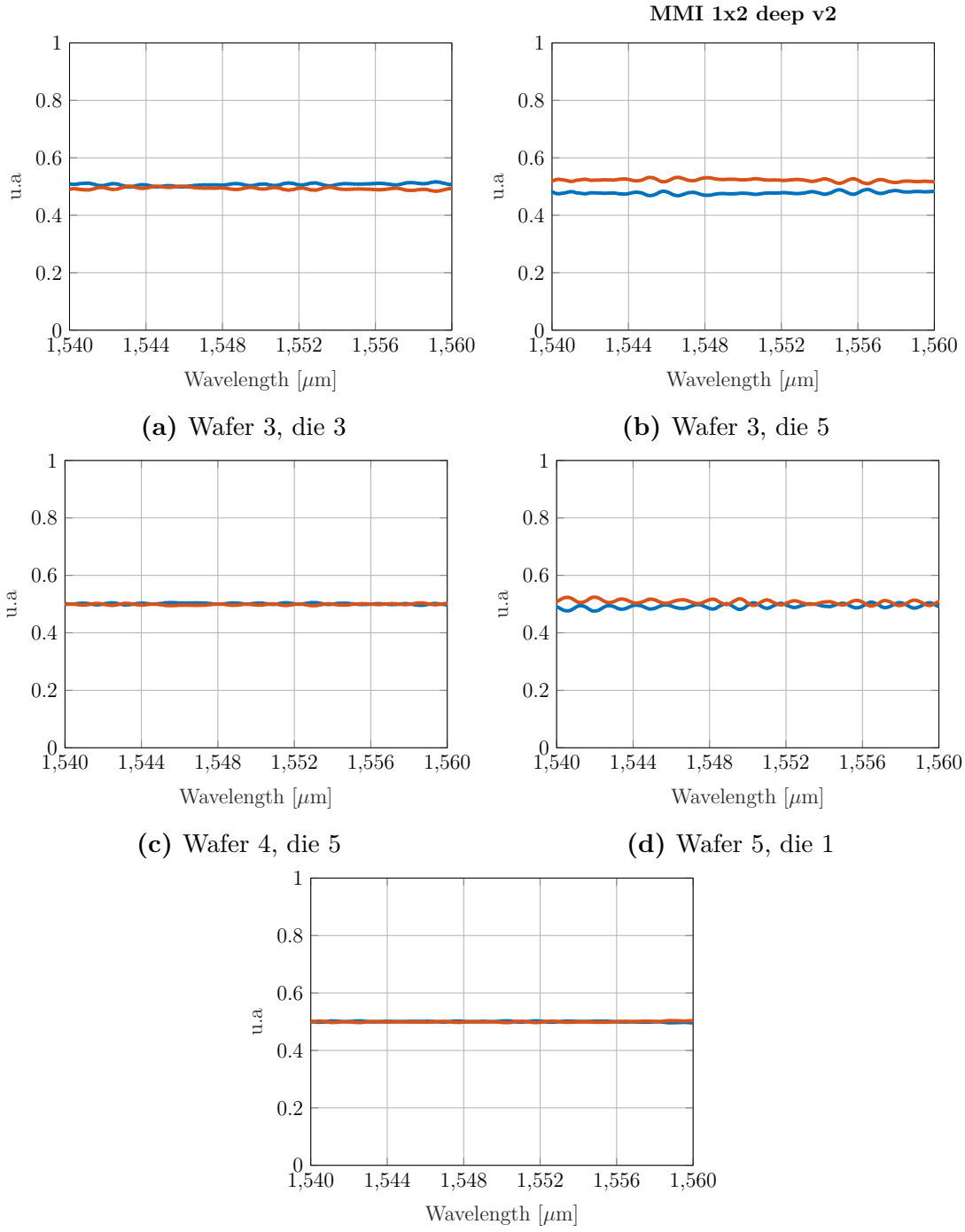

(a) Wafer 3, die 3

(b) Wafer 3, die 5

(c) Wafer 4, die 5

(d) Wafer 5, die 1

(e) Wafer 5, die 5

Figure 30: Normalized measurements the 1x2 MMI of 11.4 µm width outputs.

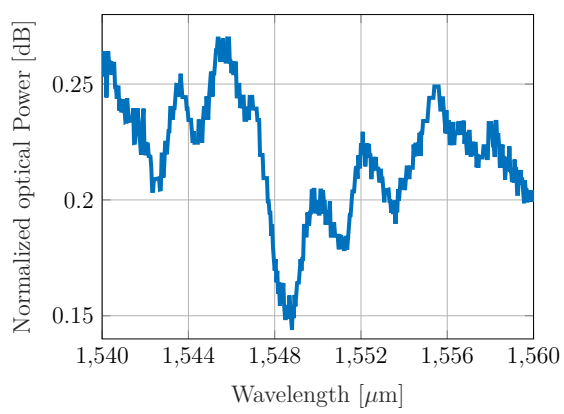

(a) Wafer 3, die 3

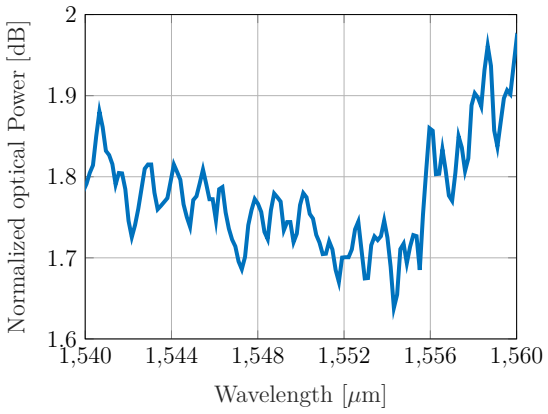

(b) Wafer 3, die 5

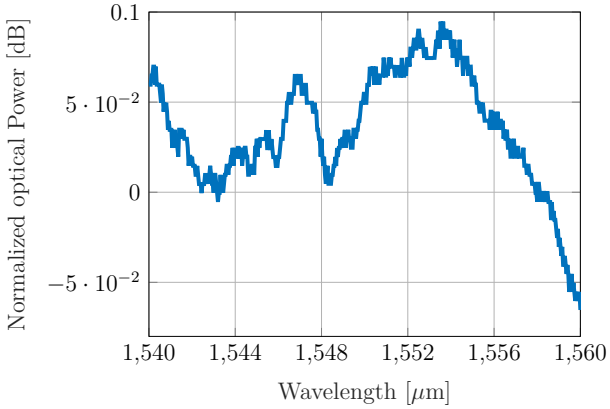

(c) Wafer 4, die 5

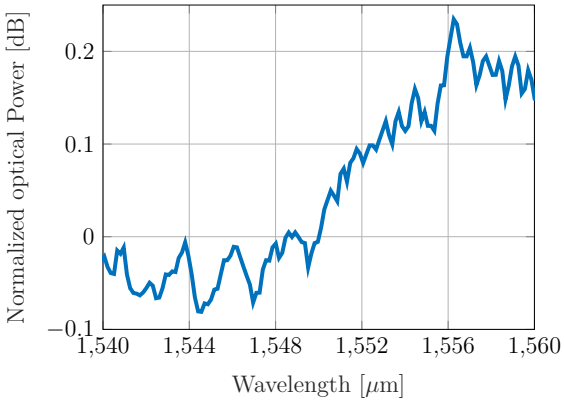

(d) Wafer 5, die 1

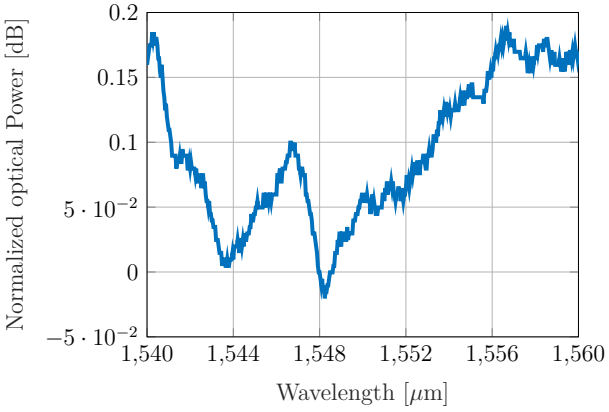

(e) Wafer 5, die 5

Figure 31: Excess losses of 1x2 MMI of 11.4 µm width.

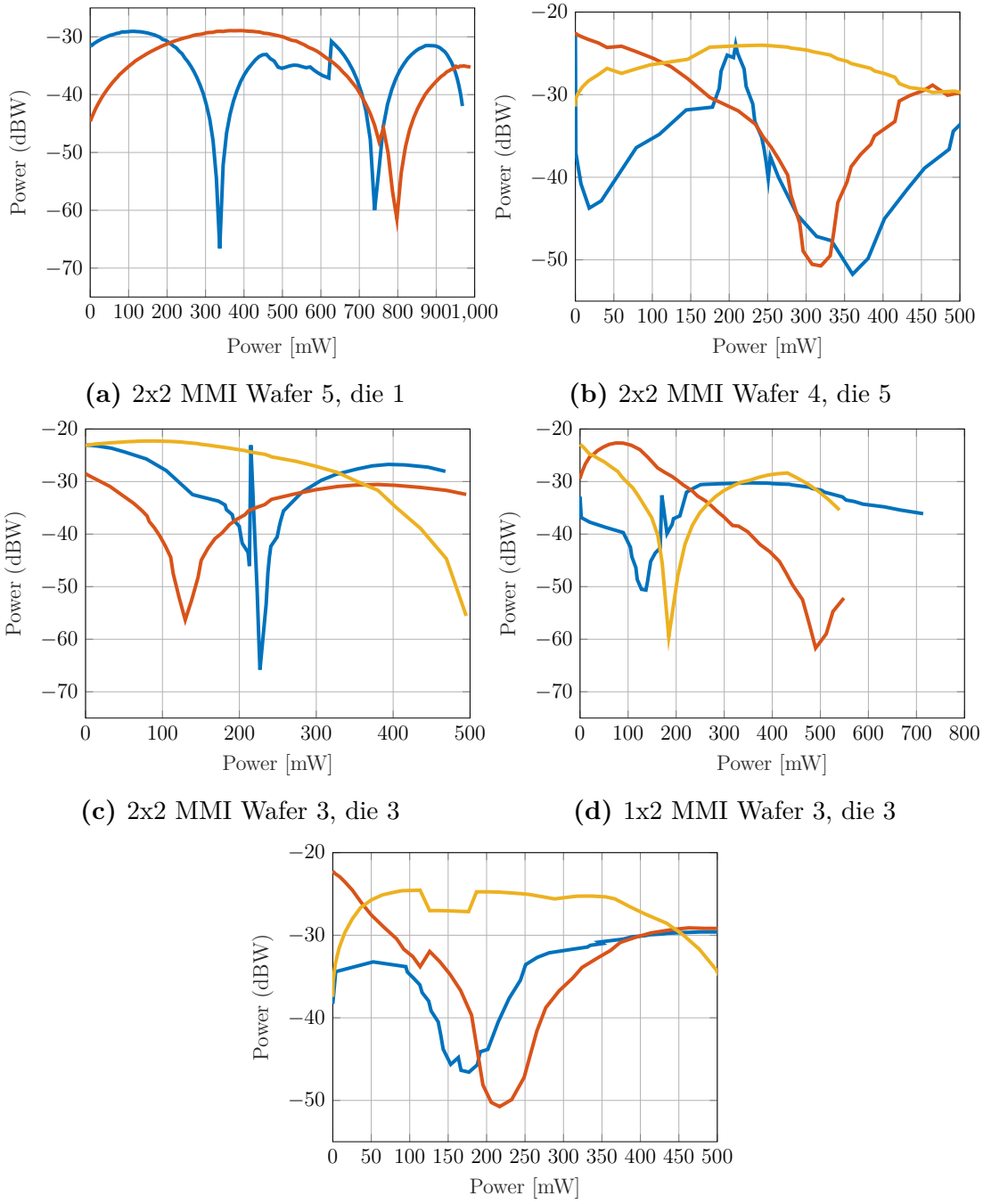

(a) 2x2 MMI Wafer 5, die 1

(b) 2x2 MMI Wafer 4, die 5

(c) 2x2 MMI Wafer 3, die 3

(d) 1x2 MMI Wafer 3, die 3

(e) 1x2 MMI Wafer 4, die 5

Figure 32: MZI versus RSL of 11.4 µm width MMIs. RSL Reflection (MMI1x2) or Transmision (MMI2x2) (blue), MZI Cross-port (red) and MZI Direct-port (yellow)

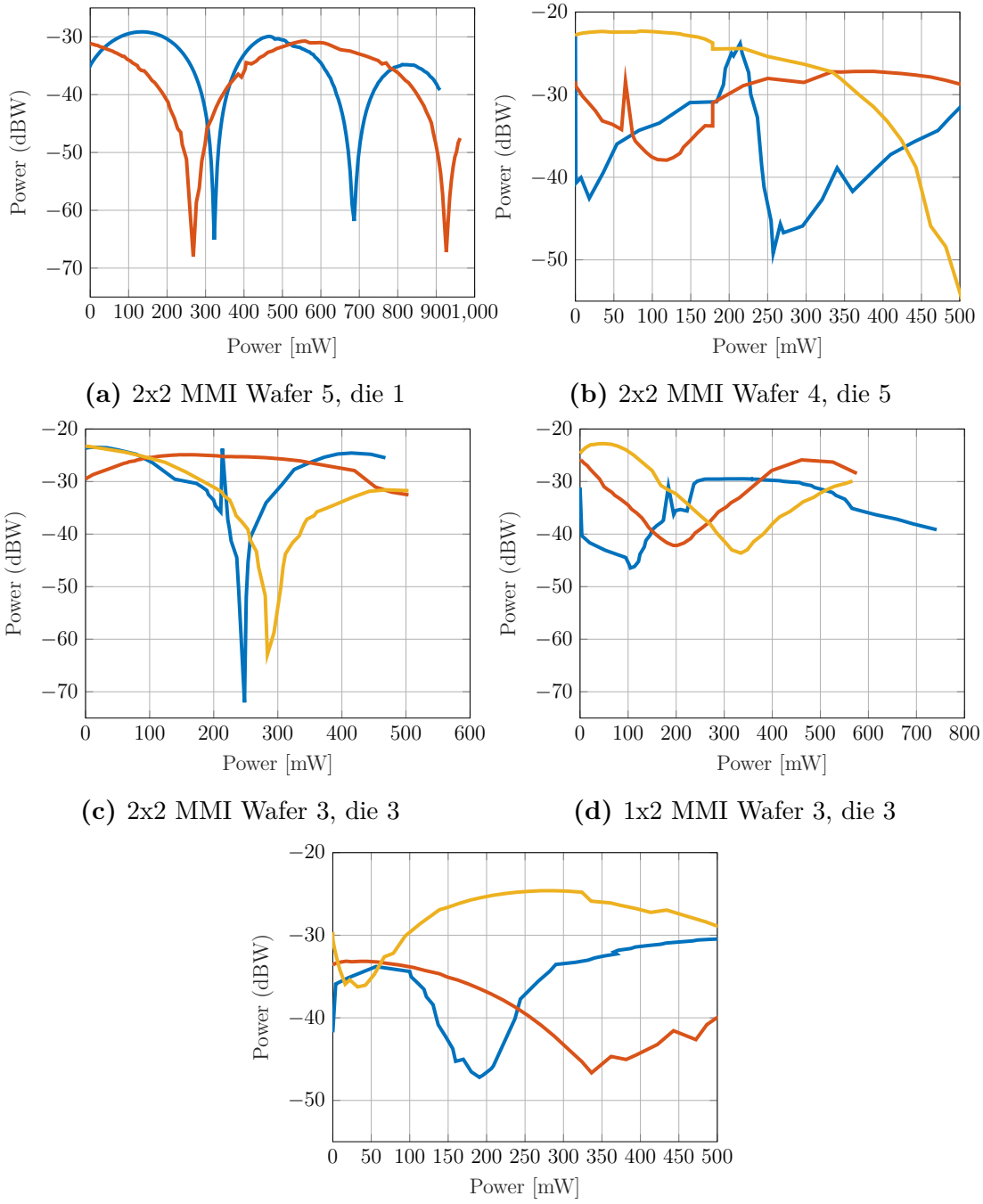

(a) 2x2 MMI Wafer 5, die 1

(b) 2x2 MMI Wafer 4, die 5

(c) 2x2 MMI Wafer 3, die 3

(d) 1x2 MMI Wafer 3, die 3

(e) 1x2 MMIWafer 4, die 5

Figure 33: MZI versus RSL of 8.4 µm width MMIs. RSL Reflection (MMI1x2) or Transmision (MMI2x2) (blue), MZI Cross-port (red) and MZI Direct-port (yellow)